Vol. 73, Part II, 2003

ISSN 0369-8211

Proceedings of the National Academy of Sciences India

SECTION A — PHYSICAL SCIENCES

National Academy of Sciences, India, Allahabad
राष्ट्रीय विज्ञान अकादमी, भारत, इलाहाबाद

The *Proceedings of the National Academy of Sciences, India,* is published in two Sections: Section A (Physical Sciences) and Section B (Biological Sciences). Four parts of each section are published annually (since 1960).

The Editorial Board in its work of examining papers received for publication is assisted, in an honorary capacity by a large number of distinguished scientists. The Academy assumes no responsibility for the statements and opinions advanced by the authors. The papers must conform strictly to the rules for publication of papers in the *Proceedings.* A total of 25 reprints is supplied free of cost to the author or authors. The authors may ask for a reasonable number of additional reprints at cost price, provided they give prior intimation while returning the proof.

Communication regarding contributions for publication in the *Proceedings,* books for review, subscriptions etc. should be sent to the Managing Editor, The National Academy of Sciences, India, 5 Lajpatrai Road, Allahabad-211 002 (India).

Annual Subscription for both Sections : Rs. 500.00; for each Section Rs. 250.00; Single Copy : Rs. 100.00. Foreign Subscription : (a) for one Section : US $100, (b) for both Sections U.S.$ 200.

(Air-Mail charges included in foreign subscription)

Co-Sponsored by C.S.T., U.P. (Lucknow)

PROCEEDINGS

OF THE

NATIONAL ACADEMY OF SCIENCES, INDIA

2003

VOL LXXIII SECTION–A PART II

Mixed ligand complexes of cobalt(II), copper(II) and zinc(II) with L-ornithine and L-glutamic acid in urea-water mixtures

M. SARATCHANDRA BABU[#] G. NAGESWARA RAO, K.V. RAMANA and M.S. PRASAD RAO*

Bio-Inorganic Chemistry Laboratories, School of Chemistry, Andhra University, Visakhapatnam-530 003, India.

[#]*Department of Chemistry, College of Engineering, Gandhi Institute of Technology and Management, Visakhapatnam-530 045, India*

Received Dec. 10, 2001; Accepted July 19, 2002

Abstract

Speciation of mixed lignad complexes of Co(II), Cu(II) and Zn(II) with L-ornithine and L-glutamic acid has been studied in varying concentrations (0-36.%) of urea-water solutions maintaining an ionic strength of 0.16 mol dm^{-3} (KCl) at 303 K. Titrations were carried out in the presence of different relative concentrations of metal (M) to L-ornithine (L) and L-glutamic acid (X) (M:L:X = 1:2:2, 1:2:4, 1:4:2) with potassium hydroxide. Stability constants of ternary complexes were refined with MINIQUAD75. The best-fit chemical models were selected based on statistical parameters and residual analysis. The species detected are $MLXH$, $MLXH_2$, $MLXH_2$ and $MLXH_3^{2+}$. The extra stability of ternary complexes compared to their binary complexes is believed to be due to electrostatic interactions of the side chains of ligands.

(**Keywords** : mixed ligand complexes/L-ornithine/L-glumamic acid/computer modeling/urea).

Introduction

The specificity and selectivity of enzyme-substrate reactions are achieved *in vivo* by manipulating the equivalent solution dielectric contant[1] at the active site. The equivalent solution dielectric constants of the active sites in bovine carobonic anydrase and carboxypeptidase were estimated to be 35 and 70, respectively. In carbonic anhydrase the binding of water (a substrate) to the zinc ion simply holds it in the correct stereochemical position suitable for attack by CO_2, where as in carboxypeptidase the binding of the substrate results in polarization thus facilitating hydrolysis. This variation is brought out by the changes in the interactions of the side chains of the protein moiety among themselves and with those of the solvent molecules. Further, intramolecular and ligand-ligand stacking interactions in mixed ligand complexes are favoured in water-organic media. Thus, the resulting reduced equivalent solution dielectric constant, at these active sites, is a consequence of solute-solvent and dipole-dipole interactions between the ligands and hence, knowledge of the equivalent solution dielectric constant at the active site can throw light on the mechanism of the reaction. As a result the protonation constants and binary metal-ligand stability constants have been studied[2-6] in DMF-water and urea-water mixtures.

The hepatic mitochondrial enzyme, ornithine aminotransferase catalyses the transfer of amino group of L-ornithine to α-oxoglutarate to form glutamic acid[7]. The enzyme serves an important metabolic function in the regulation of ornithine available for participation in the urea cycle[8,9]. Hence, in this communication we report the stability constants of ternary complexes of Co(II), Cu(II) and Zn(II) with L-ornithine and L-glutamic acid, in media of comparable dielectric constant with physiological fluids.

Materials and Method

Solutions of L-ornithine.HCl and L-glutamic acid (E Merck, Germany), Co(II)-, Cu(II)- and Zn(II)- chlorides were prepared by dissolving in triple distilled water. Urea was recrystallised twice from water and was dried at 60°C for 2 hours[10]. Stock solutions of urea was prepared by dissolving the appropriate quantity of the purified sample in water and stored frozen. The solution was never allowed to stand at room temperature continuously for more than 24 hours.

The titrations were carried out in the medium containing varying amounts of urea maintaining an ionic strength of 0.16 mol dm^{-3} with KCl at 303.0 ± 0.1 K. An ELICO LI-120 pH meter of 0.01 readability was used. The glass electrode was equilibrated in a well-stirred urea-water mixture containing inert electrolyte.

Titration of strong acid with alkali was carried out at regular intervals to check whether complete equilibrium was achieved. The calomel electrode was refilled with urea-water mixture of equivalent composition as that of the titrand. In each of the titrations the titrand consisted of mineral acid of approximately 1 mmol in a total volume of 50 cm^3. Titrations were carried out in presence of different relative concentrations of metal (M) to L-ornithine (L) and L-glutamic acid (X) (M:L:X = 1 : 2 : 2, 1 : 2 : 4, 1 : 4 : 2) with KOH. The analytical concentrations of the ingredients are given in Table 1.

Table 1 – Total initial concentrations of ingredients (in mmol) for mixed-ligand titrations in urea-water mixtures.
[KOH] = 0.4 mol dm^{-3}; V_0 = 50.0 cm^3; Temp. = 303 K
Mineral acid = 1.00 nmol; μ = 0.16 mol dm^{-3}

% W/W Urea	TMO			TLO		M:L:X
	Co(II)	Cu(II)	Zn(II)	L-ORN	L-GLU	
0.00	0.143	0.147	0.155	0.307	0.308	1:2:2
				0.307	0.616	1:2:4
				0.613	0.308	1:4:2
5.80	0.143	0.147	0.155	0.299	0.300	1:2:2
				0.299	0.600	1:2:4
				0.598	0.300	1:4:2
11.52	0.149	0.152	0.158	0.301	0.300	1:2:2
				0.301	0.600	1:2:4
				0.601	0.300	1:4:2
29.64	0.149	0.152	0.158	0.301	0.300	1:2:2
				0.301	0.600	1:2:4
				0.600	0.300	1:4:2
36.83	0.149	0.152	0.158	0.293	0.301	1:2:2
				0.293	0.601	1:2:4
				0.586	0.301	1:4:2

V_0 = Total Volume
μ = Ionic Strength
TMO = Total metal concentration
TLO = Total ligand concentration.

Table 2 – Best fit chemical models of mixed ligand complexes of M(II) with L-ornithine and L-glutamic acid in urea-water mixtures.
Experimental conditions : Temperature = 303 K, Ionic strength = 0.16 mol dm^{-3}

% W/W Urea	Log β_{mlxh}(SD)			NP	$U_{corr.}$	χ^2	R	Skewness	Kurtosis
	1111	1112	1113						
				Co(II)-ORN-GLU (pH range 2.0-8.0)					
0.00	27.07 (11)	-	35.11 (5)	120	1.484	99.84	0.029	-0.81	3.43
5.80	26.42 (9)	-	35.11 (5)	114	1.037	187.02	0.028	-1.27	6.17
11.52	25.15 (10)	-	25.77 (3)	105	4.225	45.83	0.016	-0.37	5.54
20.31	24.51 (11)	-	35.57 (3)	118	5.379	179.86	0.026	0.16	3.40
29.64	24.81 (10)	-	34.59 (3)	109	1.832	64.18	0.031	-0.59	5.97
36.83	25.81 (13)	-	34.13 (5)	131	1.365	43.54	0.035	0.33	4.63
				Cu(II)-ORN-GLU (pH range 1.7-5.8)					
0.00	24.47 (9)	29.07 (9)	32.28 (5)	131	3.956	132.762	0.015	-2.11	8.74
5.80	25.42 (11)	30.39 (14)	34.49 (8)	131	1.372	71.82	0.003	0.48	4.43
11.52	26.96 (9)	30.78 (4)	36.29 (2)	130	1.779	138.18	0.012	-084	2.09
20.31	25.59 (9)	31.41 (8)	35.14 (4)	127	2.052	58.27	0.011	0.51	2.88
29.64	27.92 (8)	32.45 (8)	34.78 (9)	128	1.664	54.44	0.010	-0.34	2.54

Table 2 Contd..

Table 2 Contd..

36.83	28.06 (7)	32.66 (2)	34.73 (4)	128	1.153	50.06	0.008	-0.16	1.93
				Zn(II)-ORN-GLU (pH range 2.0-8.0)					
0.00	24.14 (12)	27.87 (13)	34.89 (36)	139	4.430	194.16	0.017	-0.87	7.92
5.80	25.88 (14)	29.45 (11)	35.71 (5)	71	11.630	167.38	0.038	0.34	2.03
11.52	24.24 (11)	31.33 (7)	36.85 (2)	106	9.381	39.28	0.009	1.09	5.14
20.31	23.58 (13)	27.60 (21)	34.33 (4)	19	2.227	57.41	0.013	0.21	3.21
29.64	24.67 (9)	26.76 (14)	33.08 (6)	113	2.730	75.22	0.015	1.10	8.02
36.83	25.63 (8)	30.94 (5)	33.48 (6)	123	0.964	41.92	0.029	0.37	3.49

* : $U_{Corr} = \frac{U}{NP - m} \times 10^7$

Result and Discussion

A preliminary investigation of alkalimetric titrations of mixtures containing different mole ratios of L-ornithine and L-glutamic acid, in presence of mineral acid and inert electrolyte inferred that no condensed species are formed.

The formation constants[3-6] for acid-base equilibria and for those binary metal complexes of L-ornithine and L-glutamic acid were fixed in the refinement of mixed ligand stability constants in testing various chemical models using the computer program MINIQUAD75[11]. The best fit model was chosen as that with low standard deviation in formation constants and minimum U (corrected for degrees of freedom) which was corroborated by other statistical parameters like χ^2, R etc., given in Table 2. The stability constants of the complexes are found to follow the order Co(II) < Cu(II) > Zn(II).

Distribution diagrams :

A perusal of the distribution diagram (Fig. 1) reveals that at very low pH the concentration of mixed ligand complexes are less than those of protonated ligands. As the pH increased the concentrations of the ternary species increased. In the case of copper complexes the concentration of the ternary species are more than even those of the ligand species. *MLXH* and $MLXH_2^+$ showed unusual distribution patterns with increase in pH, whereas $MLXH_3^{2+}$ showed a maximum. The $MLXH_3^{2+}$ species may be assumed to be formed in all these systems according to the equilibrium.

$$M(II) + LH_3^{2+} + XH_3^+ = [M(LH_2)(XH)]^{2+} + 3H^+$$

In the pH region 3.0-5.0 ornithine and glutamic acid exist as LH_3^{2+} and XH_2, respectively[3]. These protonated ligands interact with the metal ion to form $MLXH_2^+$. The same species may also be formed due to the interaction between *MLX* and XH_2 or due to deprotonation of $MLXH_3^{2+}$

$$M(II) + LH_2^+ + XH_2 \rightleftharpoons M(LH)(XH)^+ + 2H^+$$

$$MLH^{2+} + XH_2 \rightleftharpoons MLXH_2^+ + H^+$$

$$MLXH_3^{2+} \rightleftharpoons MLXH_2^+ + H^+$$

In the same pH region (3.0-5.0), the existence of *MLXH* species can be explained based on the deprotonation of $MLXH_2^+$ species and also due to interaction of the metal ion with ligand species. Even though the deprotonation of $MLXH_2^+$ and interaction of metal ligand species lead to the formation of *MLXH* species, the tendency for the formation of MLH^{2+} species simultaneously in this pH range, results in a plateau in this region. Further, increase in *MLXH* species is noticed with increase in pH. This trend is mainly attributed to the absence of formation of *MLH* species at higher pH values where the other two factors dominate.

$$M(II) + LH_2^+ + XH_2 \rightleftharpoons M(LH)X \text{ or } ML(XH) + 3H^+$$

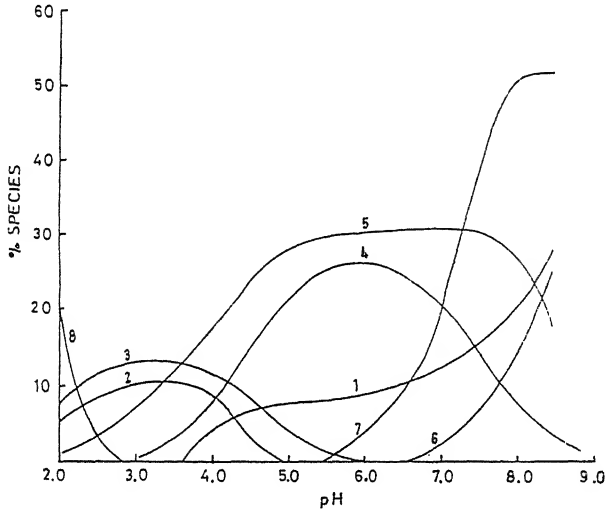

Fig. 1 –Species distribution diagrams of Co(II)-ORN-GLU :

(1) *MLXH* (2) $MLXH_3^{2+}$ (3) XH_2 (4) *XH*, (5) LH_2^+ (6) *LH* (7) X^{2-} (8) M^{2+}.

But at higher pH (5.0-8.0), MLH^{2+}, which was dominant in binary complexes, interacts with *XH* form of glutamic acid to form *MLXH*. Deprotonation of $MLXH_2^+$ also takes place producing *MLXH*.

$$MLH^{2+} + XH^- = M(LH)X + H^+$$

$$MLXH_2^+ = MLXH + H^+$$

The CuL XH_2^+ and CuLXH species are formed according to the above equilibrium at lower pH region. Hence, the plateau observed for these species in the distribution diagram for Co(II) and Zn(II) system is absent in Cu(II) system.

The concentrations of binary complexes in the presence of ternary species are less than 10% in all the systems. Hence, they are not depicted in the distribution diagrams.

Stability of ternary complexes :

The change in stability of ternary complexes as compared to their binary analogues was quantified. In one of the approaches[12,13] the difference in stability (Δ log K) for the two reactions ML with X and M (aq) with X, where X is a secondary ligand, is compared with that calculated purely on statistical grounds (Eq. 1).

$$\Delta \log K = \log K^{ML}_{MLX} - \log K^{M}_{MX} = \log K^{MX}_{MLX} - \log K^{M}_{ML} \quad (1)$$

Another approach[14] to quantify the stability of ternary complexes was based on the disproportionation constant (log X) given by the Eq. 2.

$$\log X = 2 \log K^{M}_{MLX} - \log K^{M}_{ML_2} - \log K^{M}_{MX_2} \quad (2)$$

The values of Δ log K_{1111} and log X_{1111} for the formation of ternary complexes of M (L-ornithine) (L-glutamic acid) are recorded in Table 3. Co(II) and Zn(II) form octahedral complexes with L-ornithine and L-glutamic acid. So on statistical grounds the expected Δ log K value is—0.4. Cu(II) is assumed to form square planar complexes and hence, the predicted statistical value of Δ log K is—0.6. The higher values observed in the present study infer that the ternary complexes are more stable than the binary complexes.

Table 3– Variation of stability of ternary complexes of M(II) (ornithine) (glutamic acid) in urea-water mixtures.

% W/W Urea	Co(II)		Cu(II)		Zn(II)
	Δ Log K_{1111}	Log X_{1111}	Δ Log K_{1111}	Log X_{1111}	Δ Log K_{1111}
0.00	8.38	18.53	-2.28	-0.91	4.82
5.80	792	17.58	-1.61	1.36	6.66
11.52	7.31	16.15	0.01	5.87	5.46
20.31	6.80	15.64	-1.98	2.18	5.37

Table 3 Contd.

Table 3 contd..

29.64	6.72	16.01	-0.40	6.66	5.89
36.83	8.19	17.62	1.34	8.85	6.89

$\Delta \log K_{1110} = \log \beta_{1110} - \log \beta_{1100} - \log \beta_{1010}$

$\log X_{1110} = 2 \log \beta_{1110} - \log \beta_{1200} - \log \beta_{1020}$

$\Delta \log K_{1111} = \log \beta_{1111} - \log \beta_{1101} - \log \beta_{1010}$

$\log X_{1111} = 2 \log \beta_{1111} - \log \beta_{1202} - \log \beta_{1020}$

The higher values of log X than those expected on the basis of statistical grounds (0.6) account for the extra stability of the ternary complexes. Log X_{1111} for Zn*LXH* species could not be calculated due to the absence of $ZnL_2H_2^{2+}$ species in the Zn(II)-Ornithine system in urea medium.

The extra stability of the ternary complexes are due to the interactions outside the coordination sphere. This may sometimes be the formation of hydrogen bonds between the coordinated ligands. A similar stabilizing effect may likewise be exerted by the electrostatic interactions between non-coordinated, charged groups of the ligands. Sakurai *et al.*[15-18] carried out extensive studies to establish the laws governing interactions of this nature. The higher stability associated with the Metal (L-ornithine) (L-glutamic acid) species compared to M(L-ornithine)$_2$ and M(L-glutamate)$_2$ can be explained on similar grounds. It can be attributed to the electrostatic interactions between non-coordinated charged groups like-NH_3^+ of L-ornithine and $-COO^-$ of L-glutamate (Fig. 2). The complexation of the metal with two L-amino acids acting as bidentate ligands with the resulting electrostatic interaction will result in a *MLXH* species with trans configuration.

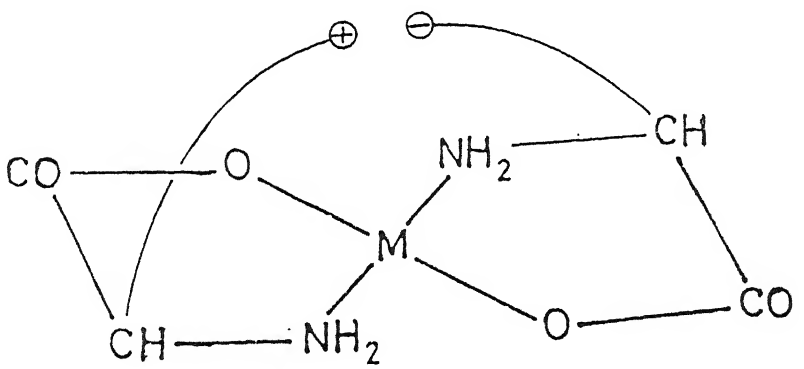

Fig. 2–*MLXH* species showing electrostatic interactions between the side chains of amino acids.

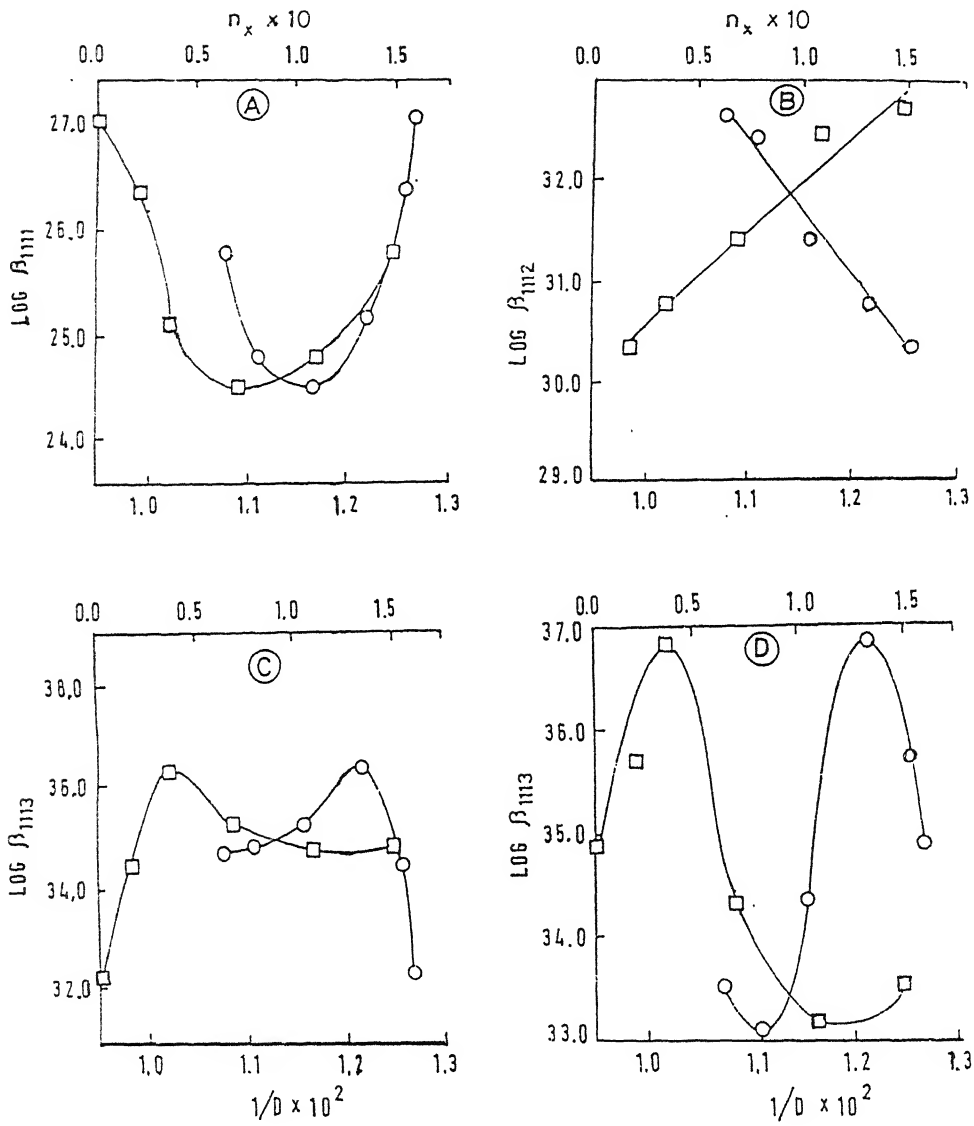

Fig. 3–Variation of log β of Co(II)-ORN-GLU (A), Cu(II)-ORN-GLU (B,C) and Zn(II)-ORN-GLU(D) with mole fraction (□-□) and reciprocal of dielectric constant (O-O) in urea-water mixtures.

Effect of urea :

Urea acts as a denaturant of macromolecules (1) by interacting with peptide groups through its amido group and (2) by breaking the water structure. The variation of stability constants with solvent parameters 1/D or n_x is shownin Fig. 3. As in the case of binary complexes, the stabilities of ternary complexes also exhibited non-linear trend with increase in urea concentration. For many of the species minima are observed at 20.31%. This trend may be due to the complete disruption of water structure brought about by urea. The non-linear and irregular variation in the stability constants of these ternary complex species may be attributed to complex solute-solvent interactions in the aqua-organic mixtures.

Conclusions

1. The species confirmed by the present study for complexes of Cu(II) and Zn(II) with L-ornithine and L-glutamic acid are $MLXH$, $MLXH_2^+$ and $MLXH_3^{2+}$. Co(II) formed only $MLXH$ and $MLXH_3^{2+}$
2. The order of the stability of these complexes was determined to be Co(II) < Cu(II) > Zn(II).
3. The concentrations of binary complexes in the presence of ternary species are less than 10% in all the system. This and the higher Δ log K and log X values observed in the study infer that the ternary complexes are more stable than the binary complexes. The higher stability of ternary complexes can be attributed to the statistical factors and electrostatic interactions between non-coordinated charged groups like $-NH_3^+$ of L-ornithine and $-COO^-$ of L-glutamate.
4. The non-linear trend of stabilities of ternary complexes with increasing urea concentration and minima at 20.31% may be due to the complete disruption of water structure brought about by urea and due to complex solute-solvent interactions in the aqua-organic mixtures.

References

1. Sigel H., Martin, R. B., Tribolet, R., Haring, U.K. & Malini R. B. (1985) *Eur. J. Biochem.* **152** : 187.
2. Babu M. S., Sukumar, J. S., Rao G. N. & Rao, M. S. P. (1995) *Indian J. Chem.* **34-A** : 567.
3. Babu M. S., Sukumar, J. S., Rao G. N., Rao, M. S. P. & Ramana, K. V. (1997) *J. Indian Chem. Soc.* **74** : 452.

4. Babu M. S., Rao G. N., Ramana, K. V.& Rao, M. S. P (2000) *J. Indian Chem. Soc.* **77** : 380.
5. Babu M. S., Rao G. N., Ramana, K. V.& Rao, M. S. P (2001) *Indian J. Chem. Soc.* **40-A** : 1334.
6. Babu M. S., Rao G. N., Ramana, K. V.& Rao, M. S. P (2001) *J. Indian Chem. Soc.* **78** : 280.
7. Peraino, C. & Pitot, H. C. (1963) *Biochim. Biophys. Acta.* **73** : 222.
8. Morris, J. E. & Peraino, C. (1976) *J. Biol. Chem.* **251** : 2571.
9. Boernke, W. E., Stevens, F. S. & Peraino, C. (1981) *Biochem.* **20** : 115.
10. Subramanian, S., Balasubramanian, D. & Ahluwalia, J. C. (1969) *J. Phys. Chem.* **73** : 266.
11. Gans, P., Sabatini, A. & Vacca, A. (1976) *Inorg. Chim. Acta.* **18** : 237.
12. Griesser, R. & Sigel, H. (1973) *Inorg. Chem.* **12** : 1198.
13. Griesser, R. & Sigel, H. (1974) *Inorg. Chem.* **13** : 462.
14. Martin, R. B. & Prados, R. (1974) *J. Inorg. Nucl. Chem.* **36** : 1665.
15. Sakurai, T., Yamauchi, O. & Nakahara, A. (1976) *Bull. Chem. Soc., Japan* **49** : 169.
16. Sakurai, T., Yamauchi, O. & Nakahara, A. (1976) *Bull. Chem. Soc., Japan* **49** : 1579.
17. Yamauchi, O., Sakurai, T. & Nakahara, A. (1977) *Bull. Chem. Soc., Japan* **50** : 1776.
18. Sakurai, T., Yamauchi, O. & Nakahara, A. (1978) *Bull. Chem. Soc., Japan* **51** : 3203.

PROC. NAT. ACAD. SCI. INDIA, 73 (A), II, 2003

Thermal decomposition of caesium bis-oxalatodiaquaindate(III) monohydrate

TESFAHUN KEBEDE, B. B. V. SAILAJA, KARRI V. RAMANA and M.S.PRASADA RAO*

Bio-inorganic Chemistry Laboratories, School of Chemistry, Andhra University, Visakhapatnam, India.

Received December 13, 2001; Revised April 27, 2002; Accepted July 19, 2002

Abstract

Indium(III) is precipitated with oxalic acid in the presence of excess caesium sulphate maintaining In^{3+} : $C_2O_4^{2-}$ at 1:2. The chemical analysis of the complex salt obtained corresponds to the formula, $Cs[In(C_2O_4)_2(H_2O)_2].H_2O$. Thermal decomposition studies show that the compound decomposes first to the anhydrous caesium indium oxalate and then to the final mixture of the oxides through formation of caesium carbonate and indium(III) oxide as intermediates. Isothermal study, X-ray diffraction pattern and IR spectral data support the proposed thermal decomposition mechanism.

(**Keywords**: thermal analysis / bis-oxalates / indium(III) / caesium salt / X-ray diffraction / IR data)

Introduction

The thermal decomposition of the oxalates of some transition metal ions and lanthanides were investigated by several workers[1-6]. The presence of suitable concentration of oxalates of NH_4^+, K^+, and Cs^+ resulted in the precipitation of the corresponding complex salts with indium(III) solutions[7-10]. The same precipitates were also obtained when indium(III) was titrated directly with oxalic acid in the presence of sufficient mono-, di- and tri-valent cations[11]. Studies on the complex formation of the In(III)-$H_2C_2O_4$-H_2O system carried out by pH metric[11], potentiometric[12] and solubility methods[13] indicated that the $[In(C_2O_4)_2]^-$ species is predominant in the pH range of 2-5. A solid precipitate is, therefore, obvious if sufficient precipitating cation is introduced to such a system. The present paper deals with the preparation and thermal decomposition studies of the caesium bis-oxalatodiaquaindate(III). The complex and its intermediate products of thermal

decomposition are characterised using chemical and thermal analyses, infrared absorption spectra and X-ray diffraction data.

Materials and Method

Thermal analysis unit : SEIKO combined thermal analysis system (TG/DTA-32), temperature programmable thermal balance, made in Japan and platinum crucible as container were used for taking thermograms in air. The rate of heating is fixed to 10^0C/min, and sensitivity of the instrument is 0.1 mg.

Infrared spectra : The infrared spectra of the complexes are recorded on SHIMADZU FTIR-8201 PC Infrared Spectrophotometer in KBr pellets.

X-ray diffraction data : X-ray diffractometer of RICH SEIFERT & CO.(Made in Germany) attached to a microprocessor is used for taking X-ray diffraction patterns at wave length of Cu $K_{\alpha 1}$ = 1.540598 Å.

The effect of variation of concentration of caesium sulphate was studied on the titration of indium(III) with oxalic acid in aqueous medium. It was found that the caesium bis-oxalatodiaquaindate(III) complex gets precipitated when the concentration of Cs^+ is ten times or more than that of In^{3+} at the $C_2O_4^{2-}$/ In^{3+} ratio of 2. Under these conditions the complex was prepared:

About 50 cm^3 of 0.05 M indium(III) sulphate was taken in a 400 cm^3 beaker to which about 50 cm^3 0.5M caesium sulphate and 100 cm^3 triple distilled water were added slowly while stirring the contents. Then about 50 cm^3, 0.1 M oxalic acid was added very slowly (drop wise from a burette) while stirring the contents vigorously. The complex salt formed was allowed to settle and filtered through a G_4 sintered glass crucible, washed with acidulated water (with H_2SO_4) to free it from excess of oxalic acid, and dried in a vacuum desiccator over silica gel.

The compound was analysed for its indium, oxalate and water content. Indium(III) was estimated complexometrically using 1-(2-pyridyalazo)-2-naphthol(PAN) as indicator[14] and oxalate by volumetric titration with standardised cerium(IV) sulpahate[15]. Water content was determined by difference and from thermal data. The results of the analyses are shown in Table 1.

Table 1–Chemical analysis data of caesium bis-oxalatodiaquaindate(III)

Methods of Preparation	Composition (%)			Total water	Ratio $C_2O_4^{2-}/In^{3+}$	Possible Formula
	In^{3+}	$C_2O_4^{2-}$	Cs^+			
Deichman[2]	---	---	---			$Cs[In(C_2O_4)_2].nH_2O$
Present work	23.82	37.63	27.54*	11.02*	2.06	$Cs[In(C_2O_4)_2].3H_2O$ $Cs[In(C_2O_4)_2(H_2O)_2].H_2O$
Calculated	24.03	36.85	27.83	11.30	2.00	$Cs[In(C_2O_4)_2].3H_2O$

* Calculated from the formula

Results and Discussion

Thermal Analysis :

Thermogravimetric Analysis (TGA) : The thermogram of caesium bis-oxalatodiaquaindate(III) monohydrate and the data obtained from it are shown in Fig. 1 and Table 2 respectively. The first loss, which occurs from 30° to 100°C, equals to 3.77% of the original weight of the complex (observed value is 3.88%) and corresponds to the loss of crystal water. This is followed by the complete dehydration of the complex salt to give caesium indium oxalate upto ~215°C. The observed weight loss is 11.33% against the calculated value of 11.30% for the total dehydration of the complex. This complex salt eventually exhibits complete dehydration up to around 200°C. The anhydrous salt remains relatively stable between 200° and 280°C.

Table 2–Summary of the thermal decomposition of the caesium salt

Wt. of Comp.	Step No.	Temperature		Loss in weight		Possible Decomposition product (Intermediate)
		start °C	end °C	Obs. %	Calcu. %	
12.3 mg	1.	30.0	97.3	3.88	3.77	$Cs[In(C_2O_4)_2(H_2O)_2]$
	2.	150.0	214.5	11.33	11.30	$CsIn(C_2O_4)_2 + CS[In(C_2O_4)]$
	3.	214.5	372.9	33.87	33.89	$Cs_2C_2O_4 + In_2O_3$
	4.	372.9	418.5	35.03	36.82	$Cs_2CO_3 + In_2O_3$

The decomposition of the intermediate(the anhydrous salt) takes place between 215^0 and 370^{0}C to give rise to a mixture of caesium oxalate and indium(III) oxide. Of course, the actual reaction in this temperature range is none other than the decarboxylation of the indium(III) oxalate which appears to be formed from the anhydrous intermediate along with caesium oxalate. The next stage is however, the decomposition of the caesium oxalate to the carbonate, which occurs between 370^0 and 420^{0}C. The product at this point is a mixture of Cs_2CO_3 and In_2O_3 that remains stable up to nearly 780^{0}C. The above data is in accordance with the results of the earlier study[16].

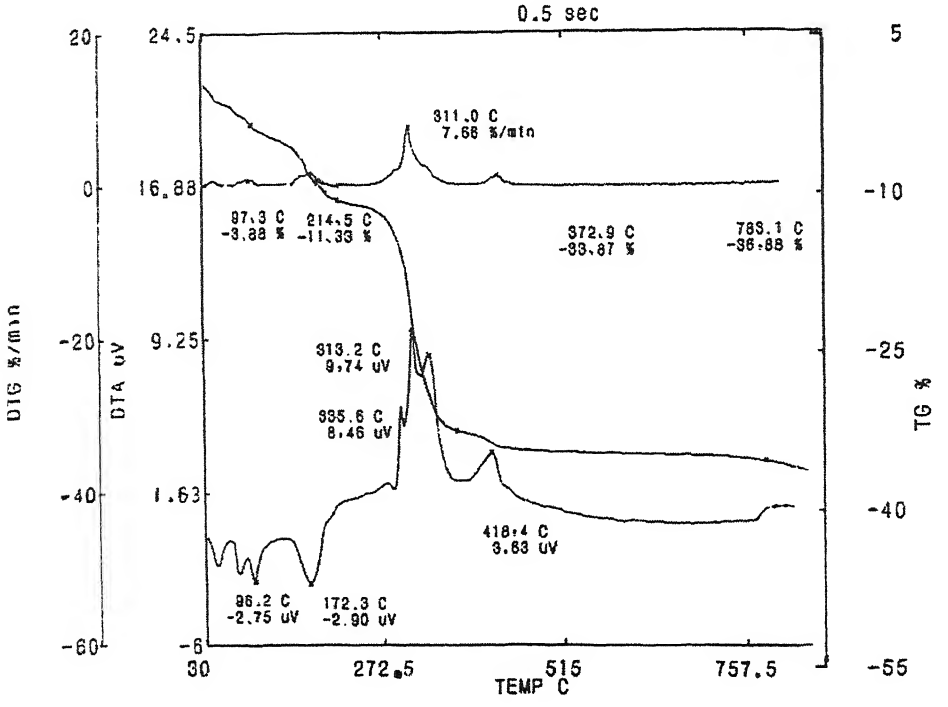

Fig. 1–TG/DTA curve of caesium bis-oxalatodiaquaindate(III) monohydrate

Differential Thermogravimetric Analysis (DTG) : Differential losses in weight obtained at regular time intervals are noted against temperature for caesium bis-oxalatodiaquaindate(III) monohydrate complex as shown in Fig. 1. The losses corresponding to the dehydrations of the complex are obvious from the small peaks at

approximately 95°C and 170°C. The broad peak with a maximum at 311.0°C, covering a range of temperature from 290° to 346°C, corresponds to the decomposition of the anhydrous caesium indium oxalate to a mixture of indium(III) oxide and caesium oxalate. A small peak around 410°C corresponds to the decomposition of caesium oxalate to caesium carbonate.

Differential Thermal Analysis (DTA) : From Fig. 1 it is clear that the dehydration of caesium bis-oxalatodiaquaindate(III) monohydrate takes place in steps. The endothermic peak with ΔT_{min} at ~90°C corresponds to the loss of crystal water. A relatively strong and broad peak with ΔT_{min} at 172.3°C is attributed to the complete dehydration of the complex to give the anhydrous caesium indium oxalate. The broad exothermic peak is split into three peaks having ΔT_{max} at 296.9°C, 313.2°C and 335.6°C corresponding to the step-wise decomposition of the caesium indium oxalate to give a mixture of caesium oxalate and indium(III) oxide. Another exothermic peak with ΔT_{max} at 418.4°C signifies the formation of caesium carbonate by decomposition of the oxalate. The final product is stable upto 780°C.

Isothermal decomposition of caesium bis-oxalatodiaquaindate(III) monohydrate : The thermal decomposition product of the caesium bis-oxalatodiaquaindate(III) monohydrate complex salt was obtained by heating ca. 100 mg. of the salt at a temperature of 186° C selected from the pyrolysis curve of the complex (Fig.1). The decomposition reaction may be described by the equation:

$$Cs[In(C_2O_4)_2(H_2O)_2].H_2O \xrightarrow{30\text{-}215^{\circ}C} Cs[In(C_2O_4)_2] + 3H_2O$$

The product so obtained was analysed[7,8] respectively for indium(III) and oxalate contents and the ratio of $C_2O_4^{2-}$ to In(III) was found as 2:1. The water content of the original complex was also determined as three molecules for each $Cs[In(C_2O_4)_2]$ molecule based on the experimental data. Hence, the possible formula of the caesium complex becomes $Cs[In(C_2O_4)_2(H_2O)_2].H_2O$. This is in good agreement with the proposed thermal decomposition mechanism of the complex salt given at the end of this article.

Infrared spectra of caesium bis-oxalatodiaquaindate(III) monohydrate

The infrared spectra of caesium bis-oxalatodiaquaindate(III) monohydrate and the product obtained by heating the complex to 186° C are shown in Fig. 2 and Fig. 3 respectively. A very strong peak at 3600 cm^{-1}, and a shoulder at 3477 cm^{-1} and a very

broad and strong absorption at 1611 cm^{-1} (Fig. 2) confirm the presence of water in the complex. Similar absorptions, though comparatively less intense in Fig. 3 at 3560 cm^{-1} and 1600 cm^{-1} indicate the presence of water in the heated product as well. This water in the heated product may be due to absorption of moisture from the atmospheric air. A weak absorption at 650 cm^{-1} and a shoulder at 580 cm^{-1} in both figures indicate the probable presence of crystal water in the complex as well as in the product obtained by heating the complex to 186^0 C.

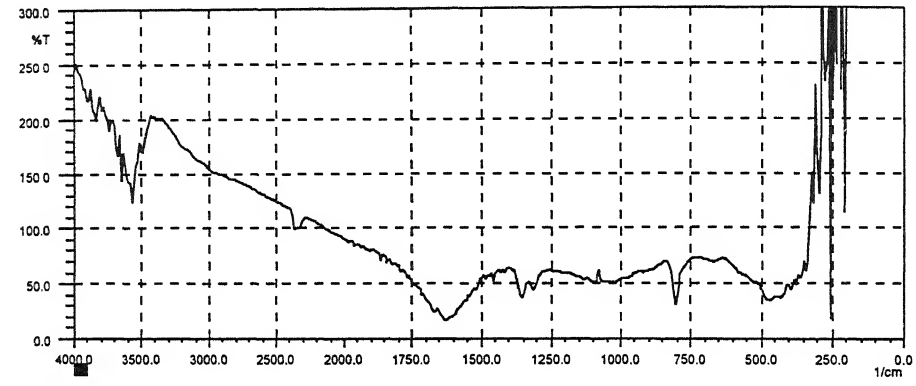

Fig. 2–Infrared spectrum of caesium bis-oxalatodiaquaindate(III) monohydrate

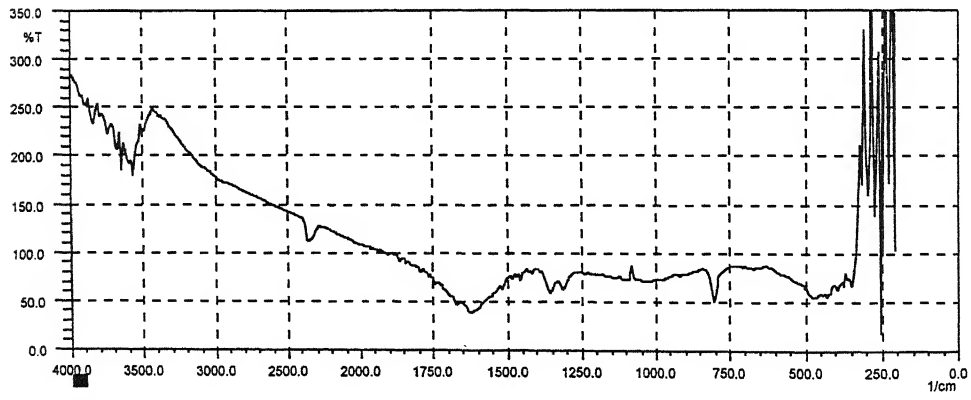

Fig. 3–Infrared spectrum of caesium bis-oxalatodiaquaindate(III) monohydrate after heating to 186^0C

A very sharp and strong absorption in the complex at 807 cm^{-1} confirms the presence of water in the coordinated form.

The comparison of the infrared spectral data of caesium bis-oxalatodiaquaindate(III) and the heated product with the empirical formula of $CsIn(C_2O_4)_2$ are shown in Table 3.

Table 3– Infrared absorption data of caesium bis-oxalatodiaquaindate(III) monohydrate and the heated product obtained at 186°C

Complex		
Original	Heated at 186°C	Band assignment
3600 sp,vs	3560 sp,vs	
3470 sh	3500 sh	$\nu_{as,s}$ (H-O-H)
	1680 sh,w	
1611 vb,vs	1620 b,s	ν_a (C=O) + δ (H-O-H)
1450 m		
1350 sp,m	1350 sp,m	ν_s (C-O) + ν (C-C)
1300 m	1300 m	ν_s (C=O) + δ (O-C=O)
810 sp,s	810 sp,s	Coordinated water & δ (O-C=O) + ν (M-O)
650 b,w		Crystal water
580 sh		
490 b,w	480 w	ν (M-O) + δ (O-C=O)
420 sh	420 sh	
350 vw	350 w	δ (O-C=O) + ν (C-C)

Key:- b = broad, m = medium, s = strong, sp = sharp, sh = shoulder, w = weak.

X-ray Diffraction Data

The X-ray diffraction data of caesium bis-oxalatodiaquaindate(III) monohydrate and that of the product obtained after heating the original complex to 186°C and cooling are given in Table 4 along with those of indium(III) oxalate for comparison.

The data in the table clearly show that the *d* spacings of the heated product does not match with the *d* spacings of $In_2(C_2O_4)_3$. So the heated product is not a mixture of indium oxalate and caesium oxalate but most probably is a single compound of caesium indium oxalate.

Table 4– X-ray diffraction data of caesium bis-oxalatodiaquaindate(III) monohydrate and the product after heating it to 186°C, compared with Indium(III) oxalate.

Cs^+ complex	Complex heated to 186°C	$In_2(C_2O_4)_3$
8.342_2		
6.836_5		5.671_3
6.395_9	6.411_x	5.515_x
6.318_7		5.357_1
6.113_5		5.092_2
5.450_8		5.035_2
4.809_3		4.794_1
4.574_3	4.654_4	4.648_1
4.505_3		4.026_2
4.281_2	4.237_4	3.921_2
4.138_2		3.807_3
3.854_4		3.677_2
3.759_2		3.555_2
3.545_2	3.531_6	3.306_1
3.498_2		3.231_2
3.470_2		3.143_1
3.380_5		3.050_4
2.806_2		3.001_2
2.769_2		2.773_1
2.737_7		2.740_2
2.711_x	2.708_5	2.529_2
2.369_2	2.398_1	2.431_2
2.334_2		2.334_2
2.308_2		2.218_1

Table 4 Contd...

Table 4 Contd...

2.241_3		2.168_1
2.135_2		2.134_1
2.069_2		2.005_2
2.047_2	2.045_4	1.952_1
1.943_4	1.950_2	1.937_2
1.919_3	1.801_1	1.840_1
1.740_4		1.779_2
		1.693_1
		1.529_1

Further the original complex was also heated to 500°C and maintained at this temperature for half an hour. The product obtained in this manner was tested for carbonate by the usual acid test. The result of this test indicates the presence of carbonate. From the thermal decomposition behavior of the complex it may be concluded that caesium carbonate is definitely formed along with the other product, indium(III) oxide

Basing on the results of the above investigations the following thermal decomposition mechanism is proposed:

$$2Cs[In(C_2O_4)_2(H_2O)_2]H_2O \xrightarrow{30°-97°C} 2Cs[In(C_2O_4)_2(H_2O)_2] \xrightarrow{150°-215C}$$

$$2CsIn(C_2O_4)_2 \xrightarrow{280°-\sim372°C} Cs_2C_2O_4+In_2O_3 \xrightarrow{\sim372°-420°C} Cs_2CO_3 + In_2O_3$$

Overall :

$$2Cs[In(C_2O_4)_2\ (H_2O)_2\ ].H_2O \longrightarrow Cs_2CO_3+In_2O_3+6H_2O+4CO+4CO_2$$

The proposed mechanism suggests the most probable structural formula of the complex with octahedral coordination around indium(III) as :

$$Cs[In(C_2O_4)_2\ (H_2O)_2\ ].H_2O.$$

Acknowledgements

One of the authors, Mr. Tesfahun Kebede, thanks the Ethiopian Embassy, New Delhi for the financial assistance.

References

1. Joseph, C., Varghese, G & Ittyachen, M.A. (1998) *J Therm. Anal. Cal.* **53** :397.
2. Chen, F., Sorensen, O.T., Meng, G & Peng, D. (1998) *J Therm. Anal. Cal.* **54** : 115.
3. Ingier-Stocka, E & Grabowska, A. (2000) *J Therm. Anal. Cal.* **62** : 285.
4. Bapat, L., Natu, G.N., Kher, J & Bhide, M (2000) *J Therm. Anal. Cal.* **62** : 295.
5. Gangadevi, T., Subba Rao, M. & Narayana Kutty, T.R. (1980) *Indian J. Chem., Sect. A,* **19** : 303.
6. Goel, S.P. & Mehrothra P.N. (1985) *Indian J. Chem., Sect. A.*, **24** : 199
7. Moeller, J.I.(1940) *J. Amer. Chem. Soc.* **62** : 2444.
8. Deichman, E.N. (1958) *Zhur. Neorg. Khim.* **3** : 1952.
9. Deichman, E.N. (1959) *Russ. J. Inorg. Chem.* 1079.
10. Deichman, E.N. (1959) *Russ. J. Inorg. Chem.* **4** : 2360.
11. Tesfahun Kebede., Sailaja, B.B.V., Nageswara Rao, G. & Prasada Rao, M.S., *J. Indian Chem. Soc.* (communicated)
12. Pingarron, J. M., Carrazon, R., Gallego Andrew & Sanchez, P. Batanero. (1984) *Bull. Soc. Chim.* Fr, 3-4, Pt. 1, 115.
13. Hasegawa, Y. & Sekine, T. (1966) *Bull. Chem. Soc.* Japan **39** : 2776.
14. Kuang, L.C. (1955) *Analyt. Chem.* **27** : 10,1582.
15. Vogel, A.I.. (1961) *'A Text Book of Quantitative Inorganic Analysis,'* Third Edition, The English Language Book Society and Longman, London, pp.320-321.
16. Sagi, S.R., Karri, V. Ramana & Prasada Rao, M.S (1980) *Indian J. Chem., Sect. A.*, **19** : 575.

PROC. NAT. ACAD. SCI. INDIA, Vol. 73, A(II), 2003

Spectrophotometric determination of five drugs in pharmaceutical formulations with chloramine-T and gallocyanine

G.P.V. MALLIKARJUNA RAO[a], P. ARUNA DEVI[a], K. M. M. KRISHNA PRASAD[a] and C.S.P. SASTRY[b]*

[a]*Department of Physical, Nuclear and Chemical Oceanography.*

[b]*Department of Organic Chemistry, Foods Drugs & Water, School of Chemistry, Andhra University, Visakhapatnam-530 003, India.*

**Author for correspondence : C.S.P. Sastry, 9-36-4, Opp. NCC Office, Andhra Bank Road, Pitapuram Colony, Visakhapatnam-530 003, India.*

Received December 21, 2001; Revised June 21, 2002; Accepted August 13, 2002

Abstract

A simple and sensitive visible spectrophotometric method has been described for the assay of clindamycin hydrochloride (CM), clomiphene citrate (CP), pimozide (PZ), mefloquine hydrochlorde (MQ) or etoposide (EPS) with excess chloromine-T (CAT) and determining the consumed CAT with a decrease in color intensity of gallocyanien (GC). All of the variables have been optimised. The concentration measurements are reproducible within a relative standard deviation of 1.0%.

(**Keywords** : clindamycin hydrocholoride/clomiphene citrate/pimozide/mefloquine hydrochloride/ etoposide/chloramine-T/gallocyanine/spectrophotometry)

Introduction

Clindamycin hydrochloride (CM)[1-4], clomiphene citrate (CP)[1-5], pimozide (PZ)[1-4], mefloquine hydrochloride (MQ)[1,3,4,6] and etoposide (EPS)[1-4] are useful as antibacterial, gonad stimulate, antipsychotic agent, antimalarial and antineoplastic agent respectively. The drugs are official in BP[1] (CM, CP, PZ, MQ and EPS), USP[2] (CM, CP, PZ and EPS) and IP[5](CP). A survey of the literature revealed that only few visible (CM[7-10], CP[11,12], PZ[13], MQ[14,15] and EPS[16,17]) and UV (CP[1,2] PZ[2] and MQ[6]) spectrophotometric methods have been reported. The reported spectrophotometric method suffer deficiencies such as low ε value. It is therefore, of interest to develop a simple and sensitive procedure with higher ε value for the determination of CM, CP,

PZ, MQ, or EPS in pure and pharmaceutical formulations. This paper describes a visible spectrophotometric method for the determination of the drug (CM, CP, PZ, MQ or EPS) by making use of its ability to react with CAT directly. Azine-dyes are well known for their high absorptivity and gallocyanine (GC) (phenoxazine-5-ium, 1-carboxy-(7-dimethyl-amino)-3, 4-didyroxy chloride : C.I. No. 51030)[18] has been utilised for estimating excess CAT in the indirect determination of bio-active compounds[18,19]. We have applied this sensitive visible spectrophotometric procedure in the determination of CM, CP, PZ, MQ or EPS in bulk sample and pharmaceutical formulations. The method involves the addition of excess CAT to drug (CM, CP, PZ, MQ, or EPS) and unreacted CAT was determined by measurement of the decrease in abosorbance of GC.

Materials and Method

A Milton Roy Spectronic 1201 UV-Visible spectrophotometer with 1 cm matched quartz cells was used for all the absorbance measurements.

All chemicals were of analytical grade and all solutions were prepared in triply distilled water. Aqueous solution of CAT (Loba, 200 μg/ml, 7.1×10^{-4}M), GC (Croma, 100 μg/ml, 2.969×10^{-4}M) and hydrochloric acid (E. Merck, 5.0 M) were prepared by dissolving the required amounts in triple distilled water.

Stock solutions of CM, CP, PZ, MQ or EPS (400 μg/ml) were prepared by dissolving 40 mg of drug (CM, CP, PZ, MQ or EPS) initially in either 10 ml of distilled water or 0.2 M NaOH (EPS), followed by dilution to 100 ml with distilled water. Stock solutions were further diluted stepwise with distilled water to give the working standard solutions.

To each of 25 ml calibrated volumetric flasks containing standard drug solution (CM : 0.5-2.5 ml, 80 μg/ml; CP : 0.5-3.0 ml, 100 μg/ml; PZ : 0.5-3.0 ml, 40 μg/ml; MQ : 0.5-3.0 ml, 100 μg/ml; EPS : 0.5-3.0 ml, 100 μg/ml), 1.25 ml of 5 M HCl and 2 ml CAT (200 μg/ml) were added and the solutions were diluted to 20ml with distlled water. After 10 min, 5 ml of GC solution (100 μg/ml) was added and mixed thoroughly and the absorbances were measured after 5 min at 540 nm against distilled water. The blank (omitting drug) and dye (omitting drug and CAT) solution were prepared in similar manner and their absorbances were measured against distilled water. The decrease in absorbance corresponding to consumed CAT and in turn to drug content was obtained by subtracting the decrease in absorbance of the test solution (dye-test) from that of the blank solution (dye-blank). The amount of drug in a sample was obtained from the Beer Lambert's plot of drug concerned.

An accurately weighed quantity of the drug formulation in the form of capsule (CM or EPS), tablet (CP, PZ or MQ) or a measure volume of injection fluid (EPS) equivalent to 40 mg were separately taken fro each drug and extracted with warm chloroform (3 × 25 ml) and filtered. The volume of the combined chloroform extract was brought to 100 ml with chloroform. The chloform extract of each drug was evaporated to dryness and the residue obtained was dissolved to prepare working sample solutions, as described in earlier and analysed as described under the procedure for pure samples.

Result and Discussion

The optimum conditions for the development of the method for each drug were established by varying parameters one at a time[20] and observing the effect produced on the absorbance of the colored species.

The method involves two steps, namely reaction of drug, (CM, CP, PZ, MQ or EPS) with an excess of CAT and the estimation of unreacted CAT using a known excess of GC. The excess GC remaining was then measured with a spectrophotometer at 540 nm. The effect of CAT concentration and acidity for different time intervals in first step and dye concentration in second step, waiting period in each step with respect to maximum sensitivity, adhrence to Beer's law, reproducibility and stability of final color were studied through control experiments. The observed optimum conditions are incorporated in the procedure recommended. the mole ratio studies revealed that each mole of the drug consumed 1.8 (CM or CP), 1.37 (MQ), 2.67 (PZ) or 1.25 (EPS) moles of CAT. The consumption of CAT by each drug under established experimental condition giving reproducible values depends upon the nature and impact of functional groups present in it.

Analytical data :

The optical characteristics such as Beer's law limits, molar absorptivity and Sandell's sensitive for these methods are given in Table 1. The precision of the method was found by measuring absorbances of six replicate samples containing known amounts of drug and the results obtained are incorporated in Table 1. Regression analysis using the method of least square was made to evaluate the slope(b), intercept (a) and correlation coefficient® for each drug (Table 1). The relative standard deviation and % range of error at 95% confidence level are also given in Table 1. The accuracy of the method for each drug was ascertained by comparing the result by proposed method and reference method (UV) statistically[20] by

t- and F-tests (Table 2). As an additional check of accuracy of the proposed method, recovery experiments were performed by adding a fixed amount of the drug to the pre analysed formulation and the results are presented in Table 2. This comparison show that there is no significant difference between the results obtained by the proposed method and those of reference. The similarly of the results is an obvious evidence that during the application of this method, the excipients that are usually present in pharmaceutical formulations do not interfere with the assay by the proposed method. Hence, the proposed method is simple, sensitive and useful for the assay of CM, CP, PZ, MQ or EPS in pure pharmaceutical formulations.

Table 1 –Optical characteristics and precision

Para meter	CM	CP	PZ	MQ	EPS
λ_{max}(nm)	540	540	540	540	540
Beer's law limits (μgml^{-1})	0.8-8.0	1-12	0.6-4.8	1-12	2-12
Sandell's sensitive ($\mu g.cm^{-2}$/0.001 absorbance unit)	0.0157	0.202	0.0105	0.118	0.0305
Molar extinction coefficient (1. $Mole^{-1}$ cm^{-1})	2.930×10^4	2.960×10^4	4.384×10^4	2.239×10^3	1.92×10^4
Relative standard deviation (%)**	0.738	0.509	0.828	0.585	0.715
% range of error (confidence limits 0.05 level)	0.775	0.535	0.869	0.614	0.748
Correlation coefficient ®	0.9999	0.9999	0.9999	0.9999	0.9999
Regression equation Y*:					
Slope (b)	6.325×10^{-3}	4.94×10^{-2}	9.5×10^{-2}	5.331×10^{-2}	3.30×10^{-2}
Intercept (a)	2.4×10^{-3}	7.33×10^{-3}	-8.66×10^{-4}	1.466×10^{-3}	-1.067×10^{-3}

* $y = a + bc$ where c is concentration

** six replicate samples

Table 2 – Analysis of pharmaceutical formulations by proposed and reference methods

Drug/Pharmaceutical formulations*	Labelled amount (mg)	Amount found**		% Recovery by proposed method***
		Proposed method	Reference method CM[Δ], CP[1,2], PZ[2] MQ[6], EPS[#]	
CM		149.75±0.42		
Capsules-I	150	F = 1.22	149.7±0.46	98.83±0.28
		t = 1.1		
		149.91±0.61		
Capsules-II	150	F = 3.17	148.89±1.09	99.94±0.41
		t = 0.55		
		148.84±0.58		
Capsules-III	150	F = 1.12	149.42±0.57	99.20±0.38
CP		49.94±0.50		
Tablets-I	50	F= 2.44	49.81±0.32	99.88±1.01
		t = 0.45		
		50.02±0.25		
Tablets-I	50	F = 4.34	50.13±0.12	100.44±0.50
		t = 0.55		
		24.97±0.097		
Tablets-III	25	F = 3.44		
		t = 1	25.05±0.18	99.90±0.38
PZ		1.98±0.114		
Tablets-I	2	F = 3.72	2.00±0.21	99.47±0.86
		t =1.5		
		2.00±0.015		
Tablets-II	2	F = 3.07	2.011±010	100.21±0.37
		t = 2.05		

Table 2 Contd..

Table 2 Contd..

			2.00±0.015		
	Tablets-III	2	F = 2.77	1.99±0.025	99.91±0.77
			t = 1.5		
MQ			250.64±0.59		
	Tablets-I	250	F = 2.27	250.97±0.89	100.2±0.23
			t = 1.86		
			248.96±1.17		
	Tablets-II	250	F = 3.14	250.38±0.66	99.58±0.47
			t = 1.96		
			249.41±0.59		
	Tablets-III	250	F = 1.171	250.38±1.01	98.82±0.225
			t = 1.31		
EPS			496.65±1.6		
	Capsules-I	500	F = 1.03	495.1±1.50	99.33±032
			t = 1.77		
			496.6±1.35		
	Capsules-II	500	F = 2.27	499.1±2.05	99.32±0.27
			t = 1.44		
			20.19±0.052		
	Injection-I	20	F = 3.77	20.20±0.1	100.98±0.26
			t = 0.21		

* Three types of capsules/tablets (CM, CP, P, MQ or EPS) from three different pharmaceutical companies.

** Average + standard deviation of six determinations; the t-and F- test values refer to comparison of the proposed methods with the reference method. Theoretical values at 95% confidence limits, t = 2.57, F = 5.05.

*** Recovery of 10 mg added to the pharmaceutical formulations (average of three determinations)

Δ Developed in laboratory for CM in 0.1N H_2SO_4 (λ_{max} 218 nm).

\# Developed in laboratory for EPS in methanol (λ_{max} 283 nm).

References

1. *British Pharmacopoeia* (1996) H. M. Stationary Office, London p. 379, 390, 613, 934, 1143.
2. *United States Pharmacopoeia* (2000), USP Convenion Inc., Rockville p. 430, 431, 444, 445, 613, 1335, 1336.
3. *Merck Index*, XII Edn. (1996) p. 2414, 2446, 3931, 5845, 7589.
4. Martindale The Complete Drug Reference (1999) 32nd edition, p. 191.1, 432.2, 532.2, 686.2, 1439.2.
5. *Indian Pharmacopoeia* (1996) Ministry of Health and Family Welfare, Govt. of India, New Delhi, p. 841.
6. Peter Lim., "*Analytical Profiles of Drug Substances*" (1985) Vol. 14, Academic Press, New York, p. 157.
7. El-Yazbi, F. A. & Blakh Salch, M. (1993) *Analyst* **118** : 577.
8. Attia, F. M. (1994) *J. Anal. Chem.* **3** : 173.
9. Amin, A. S. (1995) *Anclusin* **23** : 415.
10. Mabrouk, M. M. & Azhar, Al. (1997) *J. Pharm. Sci.* **19** : 121.
11. Ichiba, I., Morishte, M. & Yajime, T. (1988) *Chem. Pharm. Bull.* **36** : 5009.
12. Hewale Ismail (1993) *I. Anal. Lett.* **26** : 625.
13. Kelani Khediga, A., Bebawy Lories, I., Abdel Fattch, L. & Ahmad Abdel Kader, A. (1997) *Anal. Lett.* **30** : 1843.
14. Assamoi, A., Hamam, M., Castragnier, M. & Chigneou, M. (1987) *Talanta* **32** : 1015.
15. Adelusi, S. A., Oneyekavehi & Pak, A. O. (1996) *J. Sc. Ind. Res.* **39** : 22.
16. Zarapkar, S. S., Bhounsule, N. J. & Holken, U. P. (1991) *Indian Drugs* **28** : 425.
17. Zarapkar, S. S. & Vaidya, S. J. (1992) *Indian Drugs* **29** : 183.
18. Sastry, C.S.P., Rama Srinivas, K. & Krishna Prasad, K. M. M. (1996) *Talanta* **43** : 1625.
19. Lakshmi, C.S. R. & Reddy, M. N. (1998) *Talanta* **47** : 1279.
20. Massart, D. L., Vandeginste, B. G. M., Deming, S. N., Michotte, Y. & Kaufman, L. (1988) "*Chemometric : A text book*", Elseveir, Amsterdam, 293.

PROC. NAT. ACAD. SCI. INDIA, Vol. 73, A(II), 2003

Determination of stability constant of ternary-complex of copper(II) with sulphosalicylic acid and glycine by copper(II) ion-selective electrode

SUNANDA DAS* and MAHESH CHANDRA CHATTOPADHYAYA**

**C.M.P. Degree College, Allahabad-211 002, India.*

***Electrochemical Sensor Laboratory, Department of Chemistry, University of Allahabad, Allahabad-211 002, India.*

Received May 17, 2002; Accepted August 13, 2002

Abstract

Ternary complex formed by Cu(II)-sulphosalicylic acid-glycine system has been studied by Cu(II) ion-selective electrode. The value of stability constant (log K_{MLA} = 8.63) determined from the measurement of free ion concentration using the Cu(II) ion selective electrode agrees with, determined by pH-titration technique (log K_{MLA} = 8.24).

Introduction

Ion-selective electrodes have been extensively used for the determination of stability constants[1]. In this laboratory a number of electrodes have been prepared for the determination of stability constants of metal complex (1:1) in solution[2-9]. In this paper we describe our attempt to use, for the first time, the ion-selective electrode for determination of stability constants of ternary complex (1:1:1) formed by Cu(II)-sulphosalicylic acid (SSA)-glycine system. For this a precipitate based Cu(II) ion-selective electrode was prepared as per method given in the literature[7]. In order to compare the values obtained by ion-selective electrode, the system was also studied by pH-titration technique.

Materials and Method

For that preparation of electrode CuS was used as an electroactive material which was obtained by precipitating an acidic $CuCl_2$ solution by passing H_2S gas. After separating the precipitate from the solution it was washed thoroughly with water and dried at room temperature. 100 mg of dried precipitate with an equal amount of Araldite (Ciba, India) was homogenously mixed on a piece of filter paper. The paste was spread uniformly and allowed to dry in air for 24 hr to form a master disc of ~ 0.5

mm thickness. The adhering filter paper was peeled off. A disc of 1 cm diameter was cut from the master disc. This was kept immersed in 1.0 Mol dm^{-3} $CuCl_2$ solution for two days and any portion of the filter paper still adhering to the surface of the disc, was removed. The disc dried in air, served as a master membrane. The disc was fixed to one end of a glass tube (length, 5 cm) with Araldite and dried. The tube was filled with 0.1 mol dm^{-3} $CuCl_2$ solution and kept immersed in a solution of 0.01 mol dm^{-3} $CuCl_2$ for a week. An Ag-AgCl electrode was inserted through the open end of the tube for electrical contact.

A Philips H-meter (Model PR 9405 M) was used for potential measurements with a calomel electrode as an external reference electrode. Before measurements, the prepared membrane electrode was pretreated with a solution of Cu(II) ions. All the measurements were carried out at 30 ± 1°. Double distilled water was used and chemicals were of reagent grade.

The electrode assembly for the measurement of Cu-ion concentration could be expressed as

Ag, AgCl	$CuCl_2$ 0.01 mol dm^{-3}	Membrane	Sample solution	External reference electrode

For the determination of stability constant of binary as well as of ternary complexes a titration assembly was made as shown in Fig. 1. The following sets of solutions were prepared.

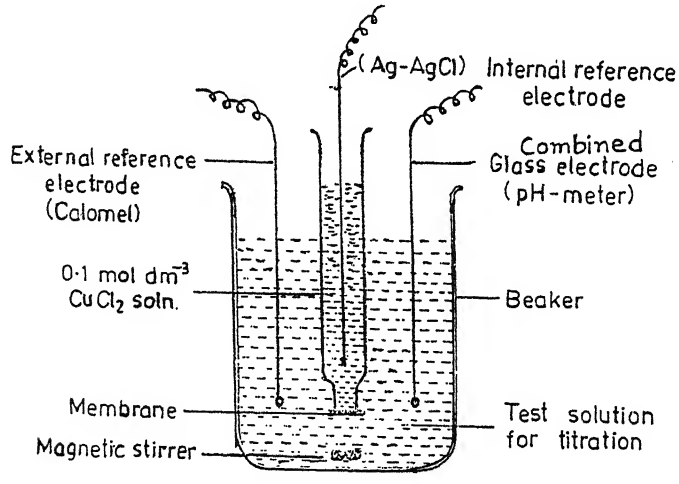

Fig. 1–A schematic representation of titration assembly.

1. Metal ion [Cu(II); 0.1 mol dm^{-3}, 2 ml] + primary ligand (sulphosalicylic acid; 0.1 mol dm^{-3}, 2 ml) + water.

2. Metal ion [Cu(II); 0.1 mol dm^{-3}, 2 ml] + secondary ligand (glycine; 0.1 mol dm^{-3}, 2 ml) + water.

3. Metal ion [Cu(II); 0.1 mol dm^{-3}, 2 ml] + primary ligand (sulphosalicylic acid; 0.1 mol dm^{-3}, 2 ml) + secondary ligand (glycine; 0.1 mol dm^{-3}, 2 ml) + water.

Since Cu(II) solution also contains an equivalent concentration of the free perchloric acid, hence in the system 1,2 and 3, perchloric acid was not added separately. Thus the concetration of free perchloric acid was kept constant in all cases.

In each case the total volume was 50 ml.

In all these sets the metal ion and ligand concentration was kept constant and pH was varied in the range of 3-6.5 by titrating it with 0.2 mol dm^{-3} of NaOH soltion. The pH and the potential of the cell were simultaneously recorded using Century CP 901 pH meter and Philips pH-meter (Model PR 9405 M) respectively at room temperature (30 ± 1°). In both the measurements a calomel electrode was used as a reference electrode.

Results and Discussion

The study of the mixed ligand complex lies in the potentiometric titration of the reaction mixture containing a 1:1:1 molar ratio of the metal, the primary ligand and secondary ligand. The metal and primary ligand as well as metal and secondary ligand containing 1:1 molar ratio of metal to ligand are also titrated pH-metrically against same alkali solution under identical conditions.

The titration curve (Fig. 2) for the binary 1:1 Cu(II)-SSA system, a well marked inflextion at a ≈ 2.0-2.5 indicating the formation of the stable [Cu-SSA] chelate. It was of interest to note that another well marked inflextion appeared at a ≈ 3. It showed the addition of extra OH and possibly formation of a dimeric species M_2A_2OH. It may also be noted that beyond a ≈ 3 (pH ~7) turbidity appears. In 1:1 Cu(II)-glycine system (MA), the titration curve gave the first inflextion at a ≈ 1, followed by a second inflextion at a ≈ 2. In this system also the turbidity appeared beyond a ≈ 2 (pH ≈ 6.5). It thus shows the formation of ML and ML(OH) respectively.

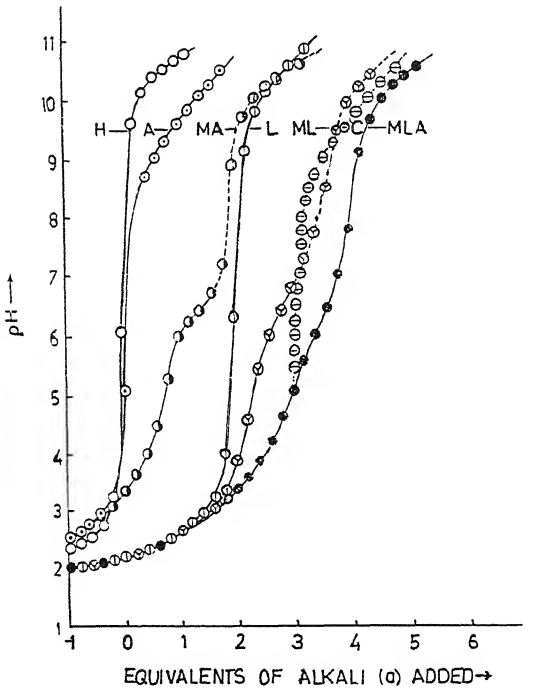

Fig. 2–Titration curves for Cu(II)-Sulphosalicylic-acid-glycine system.

H: 0.1 M $HClO_4$, A :0.1 M glycine, L : 0.1 M Sulphosalicylic acid, Cu(II) : 0.1 M.; ML: 1:1 molar ratio of Cu(II) to sulphosalicylic acid.; MA: 1:1 molar ratio of Cu(II) to glycine.; MLA : 1:1:1 molar ratio of Cu(II) to sulphosalicylic acid and glycine. ; C : Composite curve .....;.....indicates precipitation.

In 1:1:1 Cu-SSA-glycine mixed ligand system (MLA), the first inflextion occurred at a $\approx$ 4 and the solution remained clear throughout the titration. The important observations are also presented in Table 1.

Moreover the experimental mixed ligand titration curve is well displaced from the theoretical composite curve. These observations indicate the formation of the mixed ligand complex in the region a = 3-4.

Table 1– Important observation during pH titrations

System (titration curve)	Inflextion points	Color change and pH	pH of appearance of turbidity
ML	a ~ 0-2	Very light blue-	pH = 6.8
	a ~ 2-3	leafy green (pH ~ 2.9) color intensity increases.	
MA	a ~ 0-1	Light blue color intensify	no turdidity
MLA	a ~ 2-3	Very light blue-	pH = 6.8
		sea green (pH ~ 2.6)-	
		leaf green (pH ~ 3.6)-	
		bluish green (pH ~ 6.0)-	
		blue	

a = equivalents of alkali added

The reaction in the simple 1:1 Cu-SSA(ML) system may be represented as :

$$Cu^{2+} + H_2L^- \rightarrow [CuL]^- + 2H^+ \text{ at } (a = 2\text{-}2.5)$$

$$[CuL]^- + OH^- \rightarrow [CuL(OH)]^{2-} \text{ at } (a = 3)$$

The hydroxochelate may further disproportionates as

$$[CuL(OH)]^{2-} \rightarrow [CuL]^- + Cu(OH)_2$$

In the simple 1:1:1 Cu-SSA-glycine system (MLA)

$$M^{2+} + H_2L \text{ — } [ML]^- + 2H^+ \text{ at } (a = 2\text{-}3)$$

between

$$[ML]^- + HA \text{ — } [MLA]^{2-} + H^+ (a = 3\text{-}4)$$

where M^{2+} represents Cu^{2+} ion,

H_2L represents dissociated sulphosalicylic acid.

SSA represents undissociated sulphosalicylic acid.

HA represents undissociated glycine molecule.

In the region (a = 3-4), glycine combines with $[Cu\text{-}SSA]^-$ chelate to form the mixed ligand complex $[Cu\text{-}SSA\text{-}gly]^{2-}$. The result show that in 1:1:1 system, finally the mixed complex $[MLA]^{2-}$ is formed. The calculations for stability constants also support this contention. The system giving stability constant (K_{MLA}) values which agree will within experimental limits.

The protonation constant of glycine was determined by Irving and Rossotti's method[10] in aqueous medium log K_1^H = 9.14 at 30°C, which are in good agreement with those reported by Charles and Freiser[11] 9.78, whereas the dissociation constants of sulphosalicylic acid are taken from the previous work of one of the authors[12] as log K_2^H=2.93 and log K_3^H = 12.60 at 30°C.

In the present study for the potentiometric determination of stability constant of 1:1:1 mixed ligand system was calculated in terms of the secondary ligand A by the methods developed by Martell *et al.*[13,14] and Ozer[15], adopted by Singh and Srivastava[16] which is a modified form of Irving and Rossotti's method.

The binary complex formation can be shown as

$$M + H_nL \text{—} ML + nH \tag{1}$$

(charges are omitted for simplicity)

The conditional stability constant K_1 could be expressed as

$$K_1^* = \frac{[ML][H]^n}{[M][M_nL]} \tag{2}$$

However, the stability constant K_1 is defined as

$$K_1 = \frac{[ML]}{[M][L]} \tag{3}$$

$$= K_1^* \varphi$$

where,

$$K_1' = \frac{[ML]}{[M][H_nL]} = \frac{K_1^*}{[H]^n}$$

$$\text{and } \varphi = \left(1 + \frac{[H]}{Kd_1} + \frac{[H]^2}{Kd_1Kd_2} + \frac{[H]^3}{Kd_1Kd_2Kd_3} + \ldots\ldots\right) \quad (4)$$

$Kd_1Kd_2Kd_3$ ..... are first, second and third dissociation constants of ligand.

In case of sulphosaliclylic acid there are two acid groups which dissociate on complex formation and these are hydroxyl and carboxyl groups. Therefore, φ can be expressed as :

$$\varphi = \left(1 + \frac{[H]}{K_2^H} + \frac{[H]^2}{K_2^H K_3^H} + \ldots\ldots\right) \quad (5)$$

For 1:1 complex we can write

$$K_1' = \frac{[ML]}{(M^\circ - [ML])(L^\circ - [ML])} \quad (6)$$

where M° and L° are the total metal and ligand concentrations respectively.

The equation (6) can be rearranged as

$$\frac{[M]}{M^\circ - [M]} = \frac{1}{K_1'L^\circ} + \frac{[M]}{L^\circ} \quad (7)$$

Substituting K_1' from equation (3) in the equation (7) we obtain

$$\frac{[M]}{M^\circ - [M]} \cdot \frac{1}{\varphi} = \frac{1}{K_1L^\circ} + \frac{M}{\varphi} \cdot \frac{1}{L^\circ} \quad (8)$$

If the total metal and ligand concentrations are kept constant and pH of the solution is varied, a plot of $[M]/M^\circ - [M]$. $1/\varphi$ against $[M]/\varphi$ would give a straight line with slope equal to $1/L^\circ$ and intercept equal to $1/K_1L^\circ$. Thus one can calculate the value of stability constant of 1:1 complex, K_1 from the slope and intercept of such plot.

The idea could be extended further and expression for calculation of stability constant of 1:1:1 complex could be obtained. However, when 1:1:1 complex formation starts, the formation of 1:1 complex should be complete. Considered A as a secondary ligand, the formation of 1:1:1 complex can be shown to take place as

$$ML + H_nA \rightleftharpoons MLA + nH \tag{9}$$

The equilibrium constant for this reaction can be expressed as

$$K'_{1,1} = \frac{[MLA][H]^n}{[ML][H_nA]} \tag{10}$$

The stability constant for this ternary complex $K_{1,1}$ can be expressed as

$$K_{1,1} = K'_{1,1}\varphi \tag{11}$$

Where φ has same meaning as defined in equation (4) and (5) but this time the dissociation of secondary ligand A is taken into consideration.

Now the total metal ion concentration can be expressed as

$$M^{\circ} = [ML] + [MLA] + [M] \tag{12}$$

Therefore, for 1:1:1 complex, we can modify the equation (8) as

$$\frac{[M]}{\{(M^{\circ} - [ML] - [M]\}} \cdot \frac{1}{\varphi} = \frac{1}{K_{1,1}L^{\circ}} + \frac{[M]}{\phi} \cdot \frac{1}{L^{\circ}} \tag{13}$$

Thus a plot of

$$\frac{[M]}{\{(M^{\circ} - [ML] - [M]\}} \cdot \frac{1}{\varphi} \text{ against } \frac{[M]}{\varphi}$$

will give slope as 1/L and intercept as $1/K_{1,1}L^{\circ}$, from which $K_{1,1}$ can be calculated (Fig. 3).

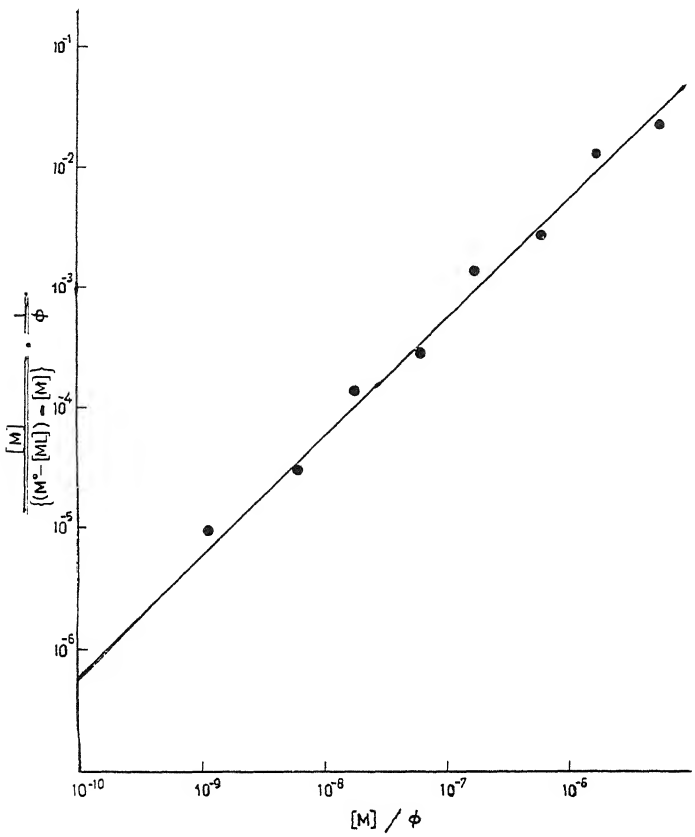

Fig. 3–Determination of stability constant of Cu(II)-SSA-glycine complex.

Plot of $\frac{M}{\{(M-[ML_1])-[M]\}}\cdot\frac{1}{\varphi}$ VS $\frac{[M]}{\varphi}$; final concn. of Cu(II) = 4×10^{-3} mol. dm^{-3},;final concn. of SSA= 4×10^{-3} mol. dm^{-3},; final concn. of glycine = 4×10^{-3} mol. dm^{-3},; pH varying, Kd_1 for glycine = 7.24×10^{-10},; temp. = 30 °C, slope = 5.08×10^{-3},; Intercept = 1.18×10^{-5}, log K_1 = 8.63.

The electrode gave a linear response down to a conc. 1×10^{-4} mol dm^{-3}. The slope of the electrode was 30 mV per decade change in concentration and this remains constant for over a period of three weeks.

To find the response time, the electrode was dipped in 0.01 mol dm^{-3} $CuCl_2$ solution and suddenly it was taken out and dipped in 0.001 mol dm^{-3} $CuCl_2$ solution.

The values of the potential change were noted every 5s. A constant potential was obtained after 30 s.

To study the effect of pH, the pH of a 0.01 mol dm^{-3} $CuCl_2$ solution was varied by the addition of NaOH or HCl. It was found that the potential remains unchanged within the pH range 3-7.5. Thus the working pH range of the electrode is 3-7.5.

The pH titration curves given in Fig. 2 reveal that sulphosalicylic acid starts forming complex much earlier than glycine and thus in the mixed complex, sulphosalicylic acid is a primary ligand and glycine is the secondary ligand.

Determination of stability constant of ternary complex using ion-selective electrode method : After obtaining the free metal concentration from the caliberation curve in the pH range 3.5-6.5, for each pH-value, the graph was plotted using the equation (12).The slope and intercept of this plot were determined by the method of least squares, which resulted in the value of stability constant (log K_{MLA}) values of 1:1:1 complex as 8.63.

Determination of stability constant by pH-titration technique : For pH titration, stability constant of ternary complex was also determined using Martell[13,14] and Ozer[15] method (log K_{MLA} = 8.24).

Thus we see that the value of stability constant of 1:1:1 complex of the ternary system Cu(II)- sulphosalicylic acid-glycine determined by ion-selective electrode (ISE) agrees quit well with the value of stability constant determined by pH titration technique. Therefore, the ion-selective electrode can be used for studying the systems where more than one ligand is attached to the metal ion.

References

1. Moddy, G.J. & Thomas, J.D.R. (1978) *Ion-Selective Electrodes in Analytical Chemistry*, Ed. Freiser, H. Plenum Press New York, Vol. 1, p. 340 and references therein.
2. Lal, U.S., Chattopadhyaya, M.C. & Dey, A.K. (1980) *J. Indian Chem. Soc.*, **19(A)** : 390.
3. Lal, U.S., Chattopadhyaya, M.C & Dey A.K. (1981) *Electrochim. Acta* **26** : 283.
4. Lal, U. S. (1982) *Doctoral Thesis*, University of Allahabad.
5. Lal, U. S., Chattopadhyaya, M.C & Dey A.K. (1982) *J. Indian Chem. Soc.* **59** : 493.
6. Bhattacharya, M. & Chattopadhyaya, M.C (1987) *J. Indian Chem. Soc.* **64** : 575.
7. Bhattacharya, M. (1992) *Doctoral Thesis*, University of Allahabad.
8. Kar, R. & Chattopadhyaya, M.C (1991) *J. Indian Chem. Soc.* **68** : 459.
9. Kar, R., Azam, N. & Chattopadhyaya, M.C (1992) *Bull Chem. Soc.*, Ethiopia **6** : 109.

10. Irving, H. & Rossotti, H. S. (1953) *J. Chem. Soc.* **3397** : (1954) 2433.
11. Charles, R. G. & Frieser, H. (1952) *J. Am. Chem. Soc.* **74**: 1385.
12. Chattopadhyaya, M.C (1974) *Doctoral Thesis*, IIT, Bombay.
13. Carey, G. H., Boguchki, R. F. & Martell, A. E. (1964) *Inorg. Chem.* **3** : 1288.
14. L. Heureux, G. A. & Martell, A. E. (1966) *J. Inorg. Nucl. Chem.* **28** : 481.
15. Ozer, O. Y. (1970) *J. Inorg. Nucl. Chem.* **32** : 1279.
16. Singh, M. K. & Srivastava, M. N. (1973) *J. Inorg. Nucl. Chem.* **35** : 2433.

PROC. NAT. ACAD. SCI. INDIA, Vol. 73, A(II), 2003

The Magic Square

JAMUNA PRASAD AMBASHT and STACEY FRANKLIN JONES*

Mathematics and Computer Science Department Benedict College, 34 Westpine Court, Columbia, SC 29212 (U.S.A)

**Computer Science Department Johns Hopkins University Baltimore, MD 21228*

Mathematics and Computer Science Department Benedict College, Columbia, SC 29204

Received July 10, 2001; Accepted January 30, 2002

Abstract

The primary purpose is to study the magic square algorithmically, but alongside passing reference to magic triangle or such relevant ideas is not ruled out. Chinese claim that the magic square was known to them as far back as 2200 B.C. The magic square was known in prehistoric days in India as found in stone carvings and inscriptions on walls and gates of old ruins. Also found in prehistoric era are some good-luck charms in business records and in horoscopes in India. Examination and construction of the magic square provides an opportunity for an aspiring mathematician and computer scientist to explore pattern generation and respective algorithm development. The magic square is also fertile ground for exploring simplification of complex arithmetic manipulation by way of algorithmic characterization.

I. Introduction

"I-King" is a Chinese classic. A numerical diagram, 'the Lo-Shu', appears in it. Emperor Yu saw, as he walked along the bank of the yellow river, a divine turtle whose back had strings of knots as shown here:

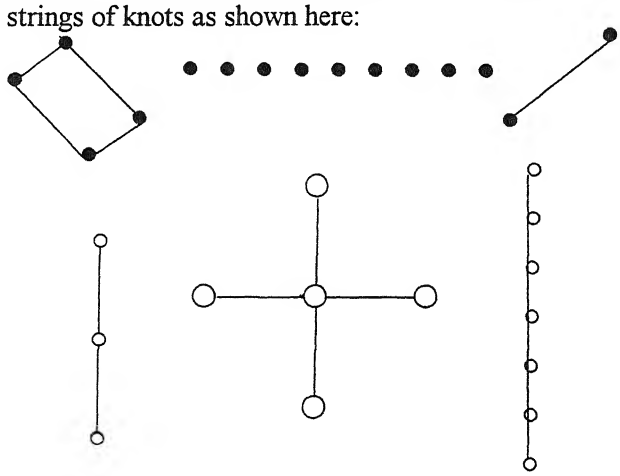

This is a 3X3 magic square

4	9	2
3	5	7
8	1	6

whose sum is15, if we add rows or columns. Interestingly enough the sums along the leading diagonals are also found to be 15. Thus a systematic study of magic squares of odd orders was undertaken. Some rules were developed.

1. The rules of arrows:
   a. Always start from the center of the top row.
   b. Extend an arrow diagonally from the top right corner of the cell and position the successive integer if possible. ↗
   c. If not, allow the arrow-head to reposition to fall to the right and straight down ↘ inside the square and position the successive integer if possible
   d. Drag the arrowhead all the way to the left corner ↖ in case (b.) is not possible; and the resulting cell at the beginning of the row was still inside the square.
   e. If the arrowhead could not follow (b.) or (c.), or whenever the arrow's movement was blocked, position the successive integer in the cell directly below the starting position.
2. The rule of bulging out:
   a. Position dotted cells in a checkered pattern on each of the four sides of the square. This creates bulges.
   b. Beginning at the left most point for each diagonal, start imaging successive integers (outside the square moving along each diagonal.)
   c. Erase the outside bulges by throwing the number inside far on the opposite side.

II. We construct a 5X5 magic square. We fix the position of 1 by using 1(a) and following the rule of arrows. This is a 5X5 normal magic square.

17	24	1	8	15
23	5	7	14	16
4	6	13	20	22
10	12	19	21	3
11	18	25	2	9

Now we construct a 5X5 magic square using the rule of bulging out.

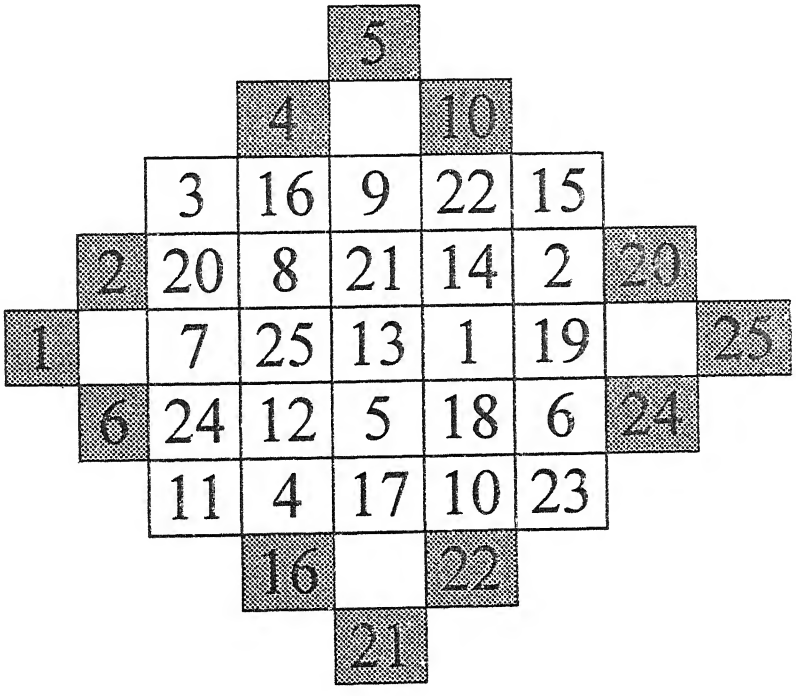

We have bulging out along the dotted lines. We follow rule outlined in 2.

III. These rules (1. and 2.) were for odd magic squares. It was found that even magic squares were much harder and sometimes impossible to construct.

Now we consider a 4X4 magic square.

16	2	3	13
5	11	10	8
9	7	6	12
4	14	15	1

FINAL ENTRY

Step 1. Cross out the leading diagonals.

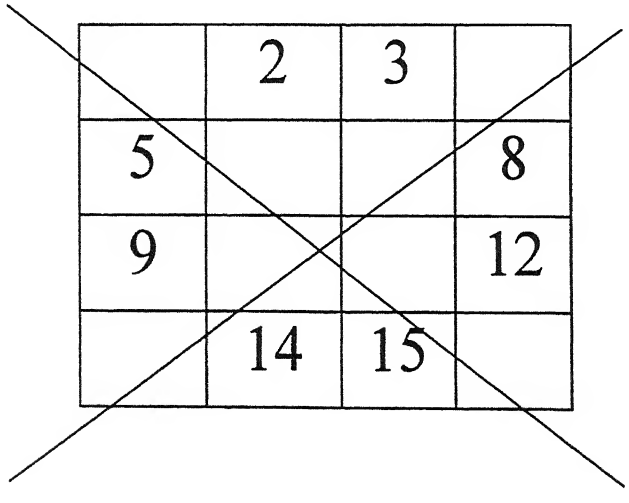

ENTRY A

Step 2. Then fill the rest.

Start filling from the bottom row to top left to right, in reverse order, and continue in this fashion with entries that were omitted.

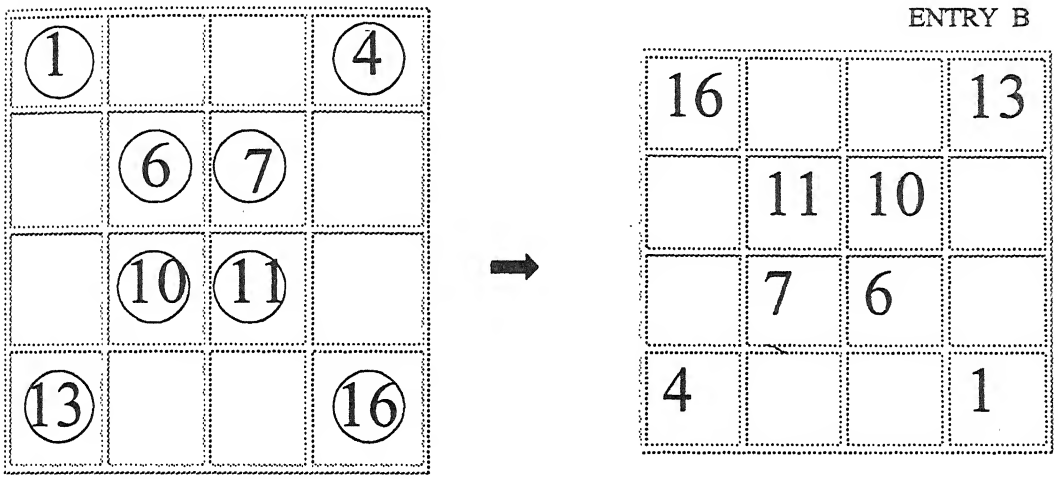

ENTRY B

Step 3. Superimpose entry B onto entry A.

IV. In this section consider an 8X8 magic square.

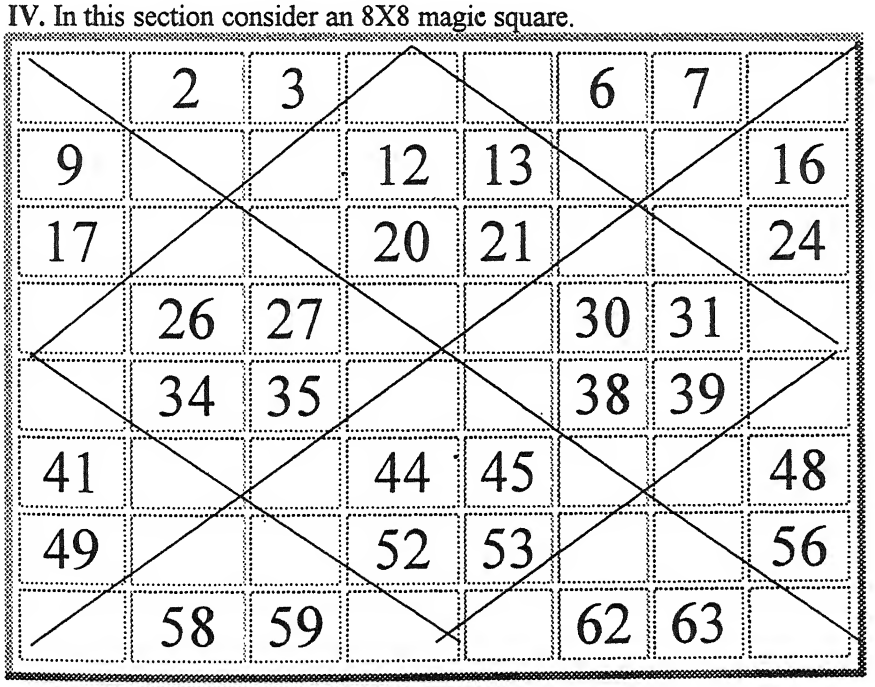

DIAGRAM A

Step 1. Cross diagonals of 4 parts of the magic square. Each part is a 4X4 grid. Start filling rows leaving blank the places where the diagonals travel. Record your blanks in a row. Superimpose diagram C on diagram A.

1			4	5			8
	10	11			14	15	
	18	19			22	23	
25			28	29			32
33			36	37			40
	42	43			46	47	
	50	51			54	55	
57			60	61			64

DIAGRAM B

64			61	60			57
	55	54			51	50	
	47	46			43	42	
40			37	36			33
32			29	28			25
	23	22			19	18	
	15	14			11	10	
8			5	4			1

DIAGRAM C

64	2	3	61	60	6	7	57
9	55	54	12	13	51	50	16
17	47	46	20	21	43	42	24
40	26	27	37	36	30	31	33
32	34	35	29	28	38	39	25
41	23	22	44	45	19	18	48
49	15	14	52	53	11	10	56
8	58	59	5	4	62	63	1

FINAL ENTRY

DIAGRAM C
SUPERIMPOSED ON
DIAGRAM A

V Consider a 12 X 12 and a 16 X 16 magic square as before.

144	2	3	141	140	6	7	137	136	10	11	133
13	131	130	16	17	127	126	20	21	123	122	24
25	119	118	28	29	115	114	32	33	111	110	36
108	38	39	105	104	42	43	101	100	46	47	97
96	50	51	93	92	54	55	89	88	58	59	85
61	83	82	64	65	79	78	68	69	75	74	72
73	71	70	76	77	67	66	80	81	63	62	84
60	86	87	57	56	90	91	53	52	94	95	49
48	98	99	45	44	102	103	41	40	106	107	37
109	35	34	112	113	31	30	116	117	27	26	120
121	23	22	124	125	19	18	128	129	15	14	132
12	134	135	9	8	138	139	5	4	142	143	1

256	2	3	253	252	6	7	249	248	10	11	245	244	14	15	241
17	239	238	20	21	235	234	24	25	231	230	28	29	227	226	32
33	223	222	36	37	219	218	40	41	215	214	44	45	211	210	48
208	50	51	205	204	54	55	201	200	58	59	197	196	62	63	193
192	66	67	189	188	70	71	185	184	74	75	181	180	78	79	177
81	175	174	84	85	171	170	88	89	167	166	92	93	163	162	96
97	159	158	100	101	155	154	104	105	151	150	108	109	147	146	112
144	114	115	141	140	118	119	137	136	122	123	133	132	126	127	129
128	130	131	125	124	134	135	121	120	138	139	117	116	142	143	113
145	111	110	148	149	107	106	152	153	103	102	156	157	99	98	160
161	95	94	164	165	91	90	168	169	87	86	172	173	83	82	176
80	178	179	77	76	182	183	73	72	186	187	69	68	190	191	65
64	194	195	61	60	198	199	57	56	202	203	53	52	206	207	49
209	47	46	212	213	43	42	216	217	39	38	220	221	35	34	224
225	31	30	228	229	27	26	232	233	23	22	236	237	19	18	240
16	242	243	13	12	246	247	9	8	250	251	5	4	254	255	1

VI. An Algorithmic Perspective

The arrow and bulging-out rules may be implemented to generate odd magic squares by an intermediate level computer scientist. Likewise the cross-diagonal elimination approach may be implemented. The focus would be on reducing the complexity and optimizing the execution in terms of time and memory. Pseudo code for the arrow rule may resemble the following:

Start at Cell (1, (n/2)+1), loop 1 to n

> Position loop value diagonally if possible using current row minus 1 and current column plus 1 as coordinates
>
> If not possible then arrow is considered blocked, then reposition to fall to theright using last row and current column plus 1 if the result falls within the square with coordinates (n,n) else position the successive integer in the cell directly below using row plus 1 and current column as coordinates

VII. Open Questions

We pose the question: Suppose n is an even number but it leaves a remainder of 2 upon dividing by 4. Is it possible to have n X n magic square in this case? To a number theorist $n \equiv 2 \pmod 4$.

VIII. Other Magic Figures

Look at the magic triangle.

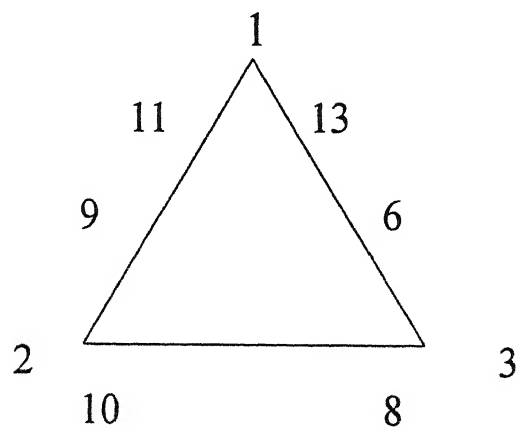

Look at the magic column.

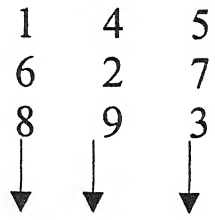

same sum

Look at the magic star.

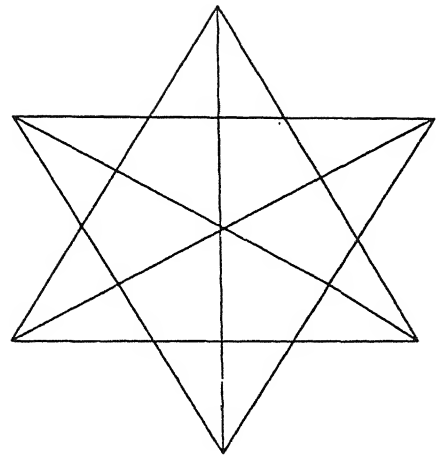

IX. What kinds of questions do the magic triangle, column and star pose? Are some of these questions passed on to us through generations through folklore?

References

1. Ball-Coxeter (1939) *Mathematics Recreations and Essays*, MacMillan.
2. Howard Eves (1983) *An Introduction to the History of Mathematics*, Saunders College Publishing, New York.

PROC. NAT. ACAD. SCI. INDIA, 73 (A), II, 2003

On multidimensional modified fractional calculus operators involving generalized Riemann Zeta function and multivariable H-function

O. P. GARG* and VIRENDRA KUMAR

M. M. H. College, Ghaziabad 201001, India.

**Address for correspondence : 111-F, 71/ 7A, Nehru Nagar, Ghaziabad, 201001, India.*

Received December 10, 2001; Accepted May 9, 2002

Abstract

In this paper, we introduce and study essentially a class of multidimensional modified fractional calculus operators involving generalized Riemann Zeta function and a general class of polynomials in the kernel. These operators are considered in the space of functions $M_\tau(R^n_+)$. Some mapping properties and fractional differential formulas are obtained . Also images of some elementary and special functions are established.

(**Keywords** : Fractional calculus operators/Mellin transform/Riemann Zeta function/General class of polynomials and multivariable H- function.)

Introduction

The H-function of r-complex variables $z_1,\ldots\ldots,z_r$ defined by Srivastava and Panda[1] by means of a multiple Mellin Barnes type contour integral is represented here in the following contracted form[2]

$$H[z_1,\ldots\ldots,z_r] = H \begin{matrix} 0,\ n : m_1,\ n_1;\ldots\ldots;m_r,n_r \\ p,\ q : p_1,\ q_1;\ldots\ldots;p_r,q_r \end{matrix}$$

$$\left[\begin{matrix} z_1 \\ \vdots \\ z_r \end{matrix}\middle|\begin{matrix} (a_j;\alpha'_j,\ldots\ldots,\alpha_j^{(r)})_1, p(c'_j,\gamma'_j)_1;\ldots\ldots\ldots\ldots;(c_j^{(r)},\gamma_j^{(r)})_1, p_r \\ (b_j;\beta'_j,\ldots\ldots,\beta_j^{(r)})_1, q : (d'_j)_1, q_1;\ldots\ldots\ldots\ldots;(d_j^{(r)},\delta_j^{(r)})_1, q_r \end{matrix}\right]$$

$$= \frac{1}{(2\pi\omega)^r} \int_{L_1} \cdots \int_{L_r} \Phi_1(\xi_1) \cdots \Phi_r(\xi_r) \psi(\xi_1, \cdots, \xi_r) z_1^{\xi_1} \cdots z_r^{\xi_r} \, d\xi_1 \cdots d\xi_r \qquad (1)$$

where $\omega = \sqrt{-1}$

For the convergence, existence conditions and other details of the above multivariable H-function, we refer to the book by Srivastava *et. al*[2].

Srivastava[3] introduced and studied a general class of polynomials which is defined by

$$S_N^M[x] = \sum_{k=0}^{[N/M]} \frac{(-N)_{MK}}{k!} A_{N,K} x^k, \qquad N = 0, 1, \ldots \qquad (2)$$

The coefficients $A_{N,K}$ $(N, k \geq 0)$ being arbitrary constants, real or complex and M is an arbitrary positive integer.

This general class of polynomials (2) unifies and extends a number of classical orthogonal polynomials such as Jacobi polynomials, Hermite polynomials, Laguerre polynomials, Gagenbauer polynomials, Bessel polynomials and several other classes of generalized hypergeometric polynomials.

Throughout this paper we use some notations. As usual R and C represent the fields of real and complex numbers respectively. R^n denotes the set of n-tuple real numbers, R_+^n non-negative real numbers and C^n complex numbers. For brevity, we write x^λ for the product $x_1^\lambda \ldots\ldots\ldots x_n^\lambda$ and x^p for $x_1^p \ldots\ldots\ldots x_n^p$ with $x = (x_1, \ldots, x_n)$, $\lambda = (\lambda_1, \ldots, \lambda_n) \in C^n$ and $p \in C$. Further we write $|\lambda|$ for the sum $\lambda_1 + \ldots\ldots + \lambda_n$. By φ_+ we mean the positive part of a function φ defined by

$$\varphi_+(x) = \begin{cases} \varphi(x), & \text{if } \varphi(x) > 0, \\ 0, & \text{if } \varphi(x) \leq 0. \end{cases} \qquad (3)$$

Goyal and Laddha[4] introduced an extension to the generalized Riemann Zeta function which is represented here in the following slightly modified form.

$$\Phi_\mu(z, s, a, n) = \sum_{n=0}^{\infty} (\mu)_n (a+n)^{-s} z^n / n!, \qquad \mu \geq 1, \ |z| < 1, \ \mathrm{Re}(a) > 0 \qquad (4)$$

obviously when $\mu = 1$ in (4), it reduces to the following generalized Zeta function[5].

$$\Phi(z,s,a) = \sum_{n=0}^{\infty} (a+n)^{-S} z^n, \qquad |z| < 1,\ \mathrm{Re}(a) > 0 \tag{5}$$

Modified fractional integrals :

The multidimensional modified fractional integral operators $\gamma_{+;n}^{\mu;N,M;s,g}$ and $\gamma_{-;n}^{\mu;N,M;s,g}$ are defined as follows

$$\gamma_{+;n}^{\mu;N,M;s,g} f(x) = \frac{1}{\Gamma(\mu+1)} \frac{\partial^n}{\partial x_1 \ldots\ldots \partial x_n} \int_{R_+^n} [\min (x_1/t_1, \ldots\ldots, x_n/t_n) - 1]_+^{\mu}$$

$$\Phi_{\omega}(z_1, s, c, g)\ S_N^M\ [z\ \{\min (x_1/t_1, \ldots\ldots, x_n/t_n) - 1\ \}^a]\ f(t)\ dt \tag{6}$$

and $$\gamma_{-;n}^{\mu;N,M;s,g} f(x) = \frac{(-1)^n}{\Gamma(\mu+1)} \frac{\partial^n}{\partial x_1 \ldots\ldots \partial x_n} \int_{R_+^n} [1 - \max (x_1/t_1, \ldots\ldots, x_n/t_n)]_+^{\mu}$$

$$\Phi_{\omega}(z_2, s, c, g)\ S_N^M\ [z\ \{1 - \max (x_1/t_1, \ldots\ldots, x_n/t_n)\}^a]\ f(t)\ dt \tag{7}$$

for $\mathrm{Re}(\mu) > 0$, where

$$z_1 = z\ \{\min (x_1/t_1, \ldots\ldots, x_n/t_n) - 1\ \}^d,\ |z_1| < 1 \tag{8}$$

and $$z_2 = z\ \{1 - \max (x_1/t_1, \ldots\ldots, x_n/t_n)\}^d,\ |z_2| < 1 \tag{9}$$

Special cases of the fractional integral operator (6) and (7) :

The fractional integral operators (6) and (7) have a large number of special cases due to the presence of the general class of polynomials and generalized Riemann Zeta function $\Phi_{\omega}(z, s, c, g)$ in the kernels of the integrals. We mention below a few of them for the sake of illustration.

(i) If we set $s = 0$ and $g = 0$ in (6) and (7) then $\Phi_{\omega}(z_1, s, c, g)$ reduces to unity and we get fractional integral operators recently studied by Goyal and Salim[6].

(ii) If we set $s = 0$, $g = 0$, $M = 1$, $N = 0$ and $A_{0,0} = 1$ in (6) and (7), then both general class of polynomials and Riemann Zeta function reduce to unity and we get the modified fractional integrals introduced by Brychkov *et. al*[7] and studied by Tuan and Saigo[8] and Raina[9].

(iii) By expressing the general class of polynomials and Riemann Zeta function involved in (6) by their series form (2) and (4) and changing order of summation and integration, we get

$$\gamma_{+;n}^{\mu;N,M;s,g} f(x) = \sum_{g=0}^{\infty} \sum_{k=0}^{[N/M]} \frac{(-N)_{Mk} A_{N,k} (\mu)_g (c+g)^{-s} z^{k+g}}{k!\, g!} \tag{10}$$

$$\frac{\Gamma(\mu+cg+ka+1)}{\Gamma(\mu+1)} X_{+}^{\mu+cg+ka} f(x)$$

(iv) if we set $n = 1$ in (6) [or in (10)], we get

$$\gamma_{+;1}^{\mu;N,M;s,g} f(x) = \sum_{g=0}^{\infty} \sum_{k=0}^{[N/M]} \frac{(-N)_{Mk} A_{N,k} (\mu)_g (c+g)^{-s} z^{k+g}}{k!\, g!} \tag{11}$$

$$\frac{\Gamma(\mu+cg+ka+1)}{\Gamma(\mu+1)} I_{+}^{\mu+cg+ka} x^{-\mu-cg-ka} f(x)$$

where I_{+}^{μ} is the well known Riemann-Liouville integral operator.

(v) on setting $\omega = 1$ $s = 1$, $M = 1$ and $A_{N,k} = \binom{N+\lambda}{N} \frac{1}{(\lambda+1)}$ in (6),

Riemann Zeta function and general class of polynomials reduce to hypergeometric function[5] and Laguerre polynmial[10] respectively and we get

$$\gamma_{+;n}^{\mu;N,1;1} f(x) = \frac{1}{c\Gamma(\mu+1)} \frac{\partial^n}{\partial x_1 \ldots\ldots \partial x_n} \int_{R_+^n} [\min\,(x_1/t_1, \ldots\ldots, x_n/t_n) - 1]_{+}^{\mu}$$

$$ {}_2F_1\,(1,\ c;\ 1+c;\ z_1)\ L_n^{(\lambda)}\ (z\{\min(x_1/t_1,\ldots\ldots,x_n,/t_n)-1\}^a)\ f(t)\ dt \qquad (12) $$

for $Re(\mu) > 0$, $|z_1| < 1$

(vi) on setting $\omega = 1$, $s = -m$ ($m = 1,2,3,\ldots\ldots$) in (6), generalized Riemann Zeta function is expressed in terms of Bernoulli's polynomial[5] and we get

$$ \gamma_{+;n}^{\mu;N,M;-m,g}\ f(x) = \frac{1}{\Gamma(\mu+1)}\ \frac{\partial^n}{\partial x_1 \ldots\ldots \partial x_n} \int_{R^n} [\min\ (x_1/t_1,\ldots\ldots,x_n,/t_n) - 1]_+^{\mu} $$

$$ \left[\frac{m!}{z_1^c}\{\log(1/z_1)\}^{-m-1} - \frac{1}{z_1^c}\sum_{g=0}^{\infty}\frac{B_{m+g+1}(c)(\log z_1)^g}{g!(m+g+1)}\right] $$

$$ S_N^M\,[z\{\min\ (x_1/t_1,\ldots\ldots,x_n,/t_n)\}^a]\ f(t)\ dt \qquad (13) $$

for $|\log z_1| < 2\pi$ and $B_{m+g+1}(c)$ is Bernoulli's polynomial.

(vii) by dividing R_+^n for a fixed $x \in R_+^n$ into n sub domains with zero- measure intersection

$$ R_+^n = \bigcup_{k=1}^{n}\ \{t \in R_+^n \mid (x_k/t_k) \le (x_j/t_j),\quad j = 1,\ldots\ldots,n\ ;\ j \ne k\ \} $$

the multidimensional fractional integral operator $\gamma_{+;n}^{\mu;N,M;s,g}$ can be expressed as a finite sum of single integrals

$$ \gamma_{+;n}^{\mu;N,M;s,g}\ f(x) = \frac{1}{\Gamma(\mu+1)}\sum_{k=1}^{n}\frac{\partial}{\partial x_k} $$

$$ \left[x_k \int_0^1 (1-t)^{\mu} t^{n-\mu-1}\Phi_{\infty}\left(z[(1/t)-1]^{\beta}, s, c, g\right) S_N^M\left[z\{(1/t)-1\}^a f(x_1 t,\ldots\ldots,x_n t)\right]dt\right] \qquad (15) $$

Similarly by dividing R_+^n into sub domains with zero- measure intersection,

$$R_+^n = \bigcup_{k=1}^{n} \{t \in R_+^n \mid (x_k/t_k) \geq (x_j/t_j),\ j = 1,\ldots\ldots,n\ ;\ j \neq k\} \qquad (16)$$

we obtain

$$\gamma_{+;n}^{\mu;N,M;s,g} f(x) = \frac{-1}{\Gamma(\mu+1)} \sum_{k=1}^{n} \frac{\partial}{\partial x_k}$$

$$\left[x_k \int_1^{\infty} (t-1)^{\mu} t^{n-\mu-1} \Phi_{\infty}\left(z\left[1-(1/t)\right]^b, s, c, g\right) S_N^M\left[z\left\{1-(1/t)\right\}^a f(x_1 t, \ldots\ldots, x_n t)\right] dt \right]$$

(17

Similarly, several (known or new) results may be obtained from (7).

Modified fractional integrals of special functions :

(i) Putting $f(x) = x^d$ for $d \in c^n$ in (10) and making use of a known result [8], we get

$$\gamma_{+;n}^{\mu;N,M;s,g} x^d = \sum_{g=0}^{\infty} \sum_{k=0}^{[N/M]} \frac{(-N)_{Mk} A_{N,k} (\mu)_g (c+g)^{-s} z^{k+g}}{k!\, g!}$$

$$\frac{\Gamma(\mu + cg + ka + 1)\Gamma(n - \mu - cg - ka + |d|)}{\Gamma(\mu+1)\Gamma(n+|d|)} \qquad (18)$$

provided $Re(d_j) > -1$ $(j = 1,\ldots\ldots,n)$ and $n + Re(|d|) > \mathrm{Re}(\mu + cg + ka)$ $(k = 0,1,\ldots,[N/M])$

(ii) Set $f(x) = x^{\zeta} (ex^{\upsilon} + b)^{\lambda} H[y_1^{\rho_1} x^{\mu_1} (ex^{\upsilon} + b)^{\sigma_1}, \ldots\ldots\ldots, y_r^{\rho_r} x^{\mu_r} (ex^{\upsilon} + b)^{\sigma_r}]$ in (10). We replace multivariable H-function by its Mellin-Barnes contour integral with the help of (1), collect powers of $(ax^{\mu} + b)$ and apply the binomial expansion

$$(ax^{\mu} + b)^{\lambda} = b^{\lambda} \sum_{h=0}^{\infty} \frac{\lambda!}{h!\,(\lambda - h)!} (ax^{\mu}/b)^h \qquad (19)$$

where $(ax^{\mu}/b)<1$; prg $(ax^{\mu}/b) < \pi$

Now, collecting the powers of x and applying a known result[8] we get

$$\gamma_{+;n}^{\mu;N,M;s,g}\left\{x^{\zeta}\left(ex^{\nu}+b\right)^{\lambda}\ H\left[y_1^{\rho_1}x^{\mu_1}\left(ex^{\nu}+b\right)^{\sigma_1},\ldots\ldots,y_1^{\rho_r}x^{\mu_r}\left(ex^{\nu}+b\right)^{\alpha_r}\right]\right\}$$

$$=\sum_{g,\delta=0}^{\infty}\ \sum_{k=0}^{[N/M]}\frac{(-N)_{Mk}A_{N,k}(\mu)_g(c+g)^{-s}z^{k+g}\,\Gamma(\mu+cg+ka+1)b^{\lambda}(e/b)^{\delta}}{k!g!\delta!\,\Gamma(\mu+1)}$$

$$H^{0,n'+2:m_1',n_1';\ldots\ldots;m_r',n_r'}_{p+2,q+2:p_1,q_1;\ldots;p_r,q_r}\left[\begin{matrix}y_1^{\rho_1}x^{\mu_1}b^{\sigma_1}\\ \vdots\\ y_r^{\rho_r}x^{\mu_r}b^{\sigma_r}\end{matrix}\middle|\begin{matrix}(\lambda;\sigma_1,\ldots\ldots,\sigma_r),(1-n+\mu+cg+ka-\delta|\nu|-|\zeta|;u_1,\ldots\ldots\\ \\ (\delta+\lambda;\sigma_1,\ldots\ldots,\sigma_r),(2-n-\delta|\nu|;u_1,\ldots\ldots u_r),\end{matrix}\right.$$

$$\begin{matrix}\left(a_j;\alpha_j',\ldots\ldots,\alpha_j^{(r)}\right)_{1,p}:\left(c_j',\gamma_j'\right)_{1,p_1};\ldots\ldots\ldots\ldots;\left(c_j^{(r)},\gamma_j^{(r)}\right)_{1,p_r}\\ \left(b_j;\beta_j',\ldots\ldots,\beta_j^{(r)}\right)_{1,q}:\left(d_j',\delta_j'\right)_{1,q_1};\ldots\ldots\ldots\ldots;\left(d_j^{(r)},\delta_j^{(r)}\right)_{1,q_r}\end{matrix}\qquad(20)$$

(iii) Set $f(x) = x^{-1}H^{m',n'}_{p',q'}\left[\min\left(x_1^h,\ldots\ldots,x_n^h\right)\right]$ in (10), for $h \in R_+$, where $H(x)$ is well known

Fox's H-function[11]. For details of this function one can refer to Srivastava *et al*[2].

To evaluate the modified fractional integral of this function, we use the multidimensional Mellin inversion formula[7]:

$$f(x)=(1/2\pi i)^n\int_{(\tau)-i\infty}^{(\tau)+i\infty}f^*(s)x^{-s}\,ds \qquad(21)$$

for the Mellin transform

$$f^*(s)=M\{f(x)\}=\int_{R_+^n}x^{s-n}f(x)\,dx \qquad(22)$$

Here, and in what follows, we use the notation

$$\int_{(\tau)-i\infty}^{(\tau)+i\infty} = \int_{\tau_1-i\infty}^{\tau_1+i\infty} \cdots\cdots\cdots \int_{\tau_n-i\infty}^{\tau_n+i\infty}$$

We shall require the following known results due to Raina[9] :

$$\int_{R_+^n} x^{s-1} f\left(\min\left\{x_1^{h_1}, \ldots\ldots\ldots, x_n^{h_n}\right\}\right) dx = \frac{(-1)^{n-1}|s/h|}{s_1 \ldots\ldots s_n} f^*\left(|s/h|\right) \tag{23}$$

$Re(s_j) < 0$ $(j = 1, \ldots\ldots, n)$ and

$$\int_{R_+^n} x^{s-1} f\left(\max\left\{x_1^{h_1}, \ldots\ldots\ldots, x_n^{h_n}\right\}\right) dx = \frac{|s/h|}{s_1 \ldots\ldots s_n} f^*\left(|s/h|\right) \tag{24}$$

$Re(s_j) > 0$ $(j = 1, \ldots\ldots, n)$, where $f^*(t)$ denotes the one-dimensional Mellin transform of $f(x)$. Now, in view of (21) and by application of (23) we can express

$$x^{-1} H_{p',q'}^{m',n'}\left[\min\left(x_1^{h_1}, \ldots\ldots\ldots, x_n^{h_n}\right)\right] = \frac{(-1)^{n-1}}{h(2\pi i)^n} \int_{(\tau)-i\infty}^{(\tau)+i\infty} F^*(s) \frac{|s|}{s_1 \ldots\ldots s_n} x^{-s-1} ds \tag{25}$$

where

$$F^*(s) = \frac{\prod_{j=1}^{m'} \Gamma\left\{b_j + B_j\left(|s|/h\right)\right\} \prod_{j=1}^{n'} \Gamma\left\{1 - a_j - A_j\left(|s|/h\right)\right\}}{\prod_{j=m'+1}^{q'} \Gamma\left\{1 - b_j - B_j\left(|s|/h\right)\right\} \prod_{j=n'+1}^{p'} \Gamma\left\{a_j + A_j\left(|s|/h\right)\right\}}$$

Now operating $\gamma_{+;n}^{\mu;N,M;s,g}$ on both sides and using a known result[8] we obtain

$$\gamma_{+;n}^{\mu;N,M;s,g}\left\{x^{-1} H_{p',q'}^{m',n'}\left[\min\left(x_1^{h_1}, \ldots\ldots\ldots x_n^{n}\right)\right]\right\}$$

$$= \sum_{g=0}^{\infty} \sum_{k=0}^{[N/M]} \frac{(-N)_{Mk} A_{N,k}(\mu)_g (c+g)^{-s} z^{k+g} \Gamma(\mu + cg + ka + 1)}{k!\, g!\, \Gamma(\mu + 1)}$$

$$\frac{(-1)^{n-1}}{h(2\pi i)^n}\int_{(\tau)-i\infty}^{(\tau)+i\infty}\frac{\Gamma(-\mu-cg-ka-|s|)}{\Gamma(-|s|)}F^*(s)\frac{|s|}{s_1.....s_n}x^{-s-1} \tag{26}$$

Now , interpreting the R.H.S. of (26) as the H-function by using (25), we get

$$\gamma_{+;n}^{\mu;N,M;s,g}\left\{x^{-1}H_{p',q'}^{m',n'}\left[\min\left(x_1^h,.....\ ..x_n^n\right)\right]\right\}$$

$$=\sum_{g=0}^{\infty}\sum_{k=0}^{[N/M]}\frac{(-N)_{Mk}A_{N,k}(\mu)_g(c+g)^{-s}z^{k+g}\Gamma(\mu+cg+ka+1)}{k!g!\Gamma(\mu+1)}$$

$$x^{-1}H_{p'+1,q'+1}^{m',n'+1}\left[\min\left(x_1^h,.....,x_n^n\right)\left|\begin{matrix}(1+\mu+cg+ka,h),(a_j,A_j)_{1,p'}\\(b_j,B_j)_{1,q'},(1,h)\end{matrix}\right.\right] \tag{27}$$

provided that $\tau_j<0$ $(j=1,\ldots,n)$, $-|\tau|>\mathrm{Re}(\mu+cg+ka)>0$ $(r=0,1.....,[N/M])$; and

(i) $\Delta=\sum_{j=1}^{n'}A_j-\sum_{j=n'+1}^{p'}A_j+\sum_{j=1}^{m'}B_j-\sum_{j=m'+1}^{q'}B_j>0$, or

(ii) $\Delta=0,\ \mathrm{Re}\left(\sum_{j=1}^{p'}a_j-\sum_{j=1}^{q'}b_j\right)-(p'-q')/2+|\tau|\left(\sum_{j=1}^{p'}A_j-\sum_{j=1}^{q'}B_j\right)>1;$

$Re(a_j)<1-(|\tau|A_j/h)$ $(j=1,.....,n')$, $Re(b_j)>-|\tau|B_j/h$ $(j=1,.....,m')$,

Note that on setting $s=0$ and $g=0$ in equation (18) and (27), we get the result established by Goyal and Salim[5]. If we put $s=0$, $g=0$, $k=0$, $N=0$, $M=1$ and $A_{0,0}=1$ in equations (18) and (27), we get the results established by Tuan and Saigo[8] and by Raina[9] respectively. Moreover , if $A_j=1$ $(j=1,.....,p')$, $B_j=1$ $(j=1,.....,q')$ and $h=1$, then (27) yields the corresponding formula for Meijer's G-function obtained by Tuan and Saigo[8]

Modified fractional operators in space $M_\tau R_+^n$:

Following[8], let $M_\tau R_+^n$ denote the space of functions f which are defined on R_+^n, where $\tau = (\tau_1,\ldots, \tau_n) \in R^n$. It is proved that $f \in M_\tau\left(R_+^n\right)$, if and only if, f can be represented as the inverse Mellin transform,

$$f(x) = (1/2\pi i)^n \int_{(\tau)-i\infty}^{(\tau)+i\infty} f^*(s)x^{-s}ds \tag{28}$$

of a function $f^*(s)$ infinitely differentiable and with compact suffort on $((\tau)-i\infty, (\tau)+i\infty)$.

Theorem : Let $Re(\mu) > 0$; $\tau_j + Re(d_j) < 1$ $(j = 1,\ldots,n)$; $Re(\mu + cg + ka) + Re(\ |d|\ ) + |\tau| < n$ $(k = 0, 1,\ldots\ldots, [N/M]\ )$ for $d \in c^n$ and $\tau \in R^n$, then the operator $x^d\gamma_{+;n}^{\mu;N,M;s,g}x^{-d}$ is a homeomorphism of the space $M_\tau\left(R_+^n\right)$, onto itself.

Moreover , it can be written in the form

$$x^d\gamma_{+;n}^{\mu;N,M;s,g}x^{-d}f(x) =$$

$$\sum_{g=0}^{\infty}\sum_{k=0}^{[N/M]}\frac{(-N)_{Mk}A_{N,k}(\mu)_g(c+g)^{-s}z^{k+g}\Gamma(\mu+cg+ka+1)}{k!g!\Gamma(\mu+1)}$$

$$\frac{1}{(2\pi i)^n}\int_{(\tau)-i\infty}^{(\tau)+i\infty}\frac{\Gamma(-\mu-cg-ka-|d|-|s|+n)}{\Gamma(-|d|-|s|+n)}F^*(s)x^{-s}ds \tag{29}$$

Proof : Making use of (18), (28) and changing the order of summation and integration, we easily get (29). The interchange of order of integration is possible since $f^*(s)$ has a compact support . The function

$$\sum_{g=0}^{\infty}\sum_{k=0}^{[N/M]}\frac{(-N)_{Mk}A_{N,k}(\mu)_g(c+g)^{-s}z^{k+g}\Gamma(\mu+cg+ka+1)\Gamma(n-\mu-cg-ka-|d|-|s|)}{k!g!\Gamma(\mu+1)\Gamma(n-|d|-|s|)}$$

has compact support and is infinitely differentiable on $((\tau) - i\infty, (\tau) + i\infty)$ if so does $f^*(s)$. Hence $x^d \gamma_{+;n}^{\mu;N,M;s,g} x^{-d}$ belongs to $M_\tau\left(R_+^n\right)$. The continuity of the mapping

$f \to x^d \gamma_{+;n}^{\mu;N,M;s,g} x^{-d} f$ in $M_\tau\left(R_+^n\right)$ is obvious.

Note that on setting $g = 0$ and $s = 0$ in (29), we get the results established by Goyal and Salim[6]

Acknowledgement

The authors wish to express their sincere thanks to Dr. K. C. Gupta, M. R. Engineering College, Jaipur, India and Dr. S. P. Goyal, University of Rajasthan, Jaipur, India for the valuable suggestions given in the preparation of the present paper.

References

1. Srivastava, H. M.& Panda, R.(1976) *J. Angew Math.* **283** : 265.
2. Srivastava, H. M, Gupta, K. C. & Goyal, S. P (1982) *The H-functions of one and two variables with applications*, New Delhi- Madras : South Asian Publishers.
3. Srivastava, H. M.(1972) *Indian J. Math.* **14** : 1.
4. Goyal, S. P. & Laddha, R. K. (1997) *Ganita Sandesh.* **11** : 99.
5. Erdelyi, A. *et.al.* (1953) *Higher Transcendental Functions* ,Vol. I, McGraw-Hill, New York, Toronto and London.
6. Goyal, S. P & Salim, T. O. (1998) *Proc. Indian Acad. Sci. (Math. Sci.)* **108** : 273.
7. Brychkov, Y.A., Glaeske, H. J., Prudnikov, A. P. & Tuan,V. K. (1992) *Multidimensional integral transformations*, Philadelphia- Reading - Paris- Montreux- Tokyo- Melbourne: Gordon and Breach.
8. Tuan, V. K. & Saigo, M. (1993) *Math. Nachr.* **161** :253.
9. Raina, R. K.(1996) *Proc. Indian Acad. Sci. (Math. Sci.)* **106** :155.
10. Szego, G. (1975) *Orthogonal polynomials*, 4th Ed., Providence Rhode Island : Am. Math. Soc. Colloq. Pub.
11. Fox, C. (1961) *Trans. Am. Math. Soc.* **98** : 395.

PROC. NAT. ACAD. SCI. INDIA, 73 (A), II, 2003

Bianchi type IX string dust cosmological model in general relativity

RAJ BALI and R. D. UPADHAYA

Department of Mathematics, University of Rajasthan, Jaipur- 302004, India.

Received August 16, 2001; Revised February 1, 2002; Accepted May 20, 2002

Abstract

A Bianchi Type IX string dust cosmological model in General Relativity, is obtained. To get a determinate solution, we suppose $\varepsilon = \lambda$ and assume a transformation $d\tau = adt$ where a is function of t and a is metric potential, ε the rest energy density and λ the string tension density. The physical and geometrical aspects of the model, are also discussed.

(**Keywords** : cosmological model/relativity/bianchi type IX /string)

Introduction

The choice for the study of Bianchi type IX cosmological model creates more interest because familiar solutions like Robertson-Walker universe, the de-Sitter universe, the Taub - NUT solutions etc. are of Bianchi type IX space-time. Bianchi type IX cosmological models include closed FRW models. These models allow not only expansion but also rotation and shear and in general are anisotropic. After the big bang, cosmic strings arise during the phase transition as the temperature goes down below some critical temperature[1-3]

The general relativistic formalism of cosmic strings is due to Letelier[4,5]. Stachel[6] has investigated massless strings. Banerjee *et. al.*[7] have investigated some cosmological solutions of massive strings for Bianchi type I space-time with and without magnetic field. Chakraborty and Nandy[8] have studied Letelier strings model for Bianchi type II, VIII and IX space-time. Chakraborty[9] has also investigated a class of cosmological solution of massive strings in Bianchi type IX space-time using a supplementary conditions $a = \alpha\, b^n$ between metric potentials where a and b are functions of time-alone and α is a constant. Bali and Dave[10] have investigated some special strings solutions for Bianchi type IX space-time using the condition $\epsilon = \lambda$ and $a = e^{\alpha t}$ where a is metric potential.

In this paper, we have investigated a general string dust solution for Bianchi type IX space-time using the transformation $d\tau = a\, dt$ and the condition $\varepsilon = \lambda$ where

a is metric potential and function of t-alone, ε is the rest energy density and λ the string tension density. The physical and geometrical aspects of the model, are also discussed.

We consider the Bianchi type IX metric in the form

$$ds^2 = -dt^2 + a^2(t)\,dx^2 + b^2(t)\,dy^2 + (b^2 \sin^2 y + a^2\cos^2 y)\,dz^2$$

$$- 2a^2 \cos y\, dx\, dz \tag{1}$$

The energy momentum tensor for string dust is taken as

$$T_i^j = \varepsilon\, v_i v^j - \lambda\, x_i x^j$$

with

$$v^i v_i = -x^i x_i = -1 \tag{3}$$

and

$$v^i x_i = 0 \tag{4}$$

where $\varepsilon = \varepsilon_p + \lambda$ is the rest energy density for a cloud of strings with particles attached to them, ε_p, the density of particle, λ, the cloud strings tension density, v^i the flow velocity vector and x^i is the direction of strings.

The Einstein field equation

$$R_i^j - \frac{1}{2} R\, g_i^j = -T_i^j \tag{5}$$

[using the unit in which $\frac{8\pi G}{c^4} = 1$]

for the metric (1) leads to

$$2\frac{\dot{a}\dot{b}}{ab}+\frac{\dot{b}^2}{b^2}+\frac{1}{b^2}-\frac{1}{4}\frac{a^2}{b^4}=\varepsilon \tag{6}$$

$$2\frac{\ddot{b}}{b}+\frac{\dot{b}^2}{b^2}+\frac{1}{b^2}-\frac{3}{4}\frac{a^2}{b^4}=\lambda \tag{7}$$

$$\frac{\ddot{a}}{a}+\frac{\ddot{b}}{b}+\frac{\dot{a}\dot{b}}{ab}+\frac{1}{4}\frac{a^2}{b^4}=0 \tag{8}$$

Eqn. (6) to (8) are three eqn. in four unknowns a, b, ε and λ. To get a determinate solution, we assume

$$\varepsilon = \lambda \tag{9}$$

Subtracting (7) from (6) and using the condition given by (9), leads to

$$\frac{\dot{a}\dot{b}}{ab}-\frac{\ddot{b}}{b}+\frac{1}{4}\frac{a^2}{b^4}=0 \tag{10}$$

Again subtracting (10) from (8), we have

$$2\frac{\ddot{b}}{b}+\frac{\ddot{a}}{a}=0 \tag{11}$$

where a dot (.) denotes differentiation with respect to t.

To obtain exact solutions of (10) and (11), we make use of the scale transformation

$$d\tau = a\,dt \tag{12}$$

Using the transformation given by (12), eqn. (11) and (12) reduce to

$$\frac{b''}{b}-\frac{1}{4b^4}=0 \tag{13}$$

$$2\frac{a'b'}{ab} + 2\frac{b''}{b} + \frac{a''}{a} + \frac{a'^2}{a^2} = 0 \tag{14}$$

where a dash denotes differentiation with respects to τ.

Eqn. (13) leads to

$$\frac{d}{d\tau}\left(b'^2\right) = -\frac{1}{4}\frac{d}{d\tau}\left(\frac{1}{b^2}\right) \tag{15}$$

which on integration leads to

$$b' = \sqrt{\alpha - \frac{1}{4b^2}} \tag{16}$$

where α is the constant of integration.

Eqn. (16) further leads to

$$\frac{2b\,d\,b}{2\sqrt{\alpha}\sqrt{b^2 - \left(\frac{1}{2\sqrt{\alpha}}\right)^2}} = d\tau \tag{17}$$

using $$b^2 - \left(\frac{1}{2\sqrt{\alpha}}\right)^2 = \Im^2 \tag{18}$$

Eqn. (17) leads to

$$\frac{2\Im\, d\Im}{2\sqrt{\alpha}\Im} = d\tau \tag{19}$$

which on integration leads to

$$\Im = \sqrt{\alpha}\tau + \eta \tag{20}$$

where η is the constant of integration.

Using (18), eqn. (20) gives

$$b^2 = \alpha\tau^2 + \beta\tau + \gamma \tag{21}$$

where $$\beta = 2\sqrt{\alpha}\,\eta \tag{22}$$

$$\gamma = \left[\eta^2 + \left(\frac{1}{2\sqrt{\alpha}}\right)^2\right] \tag{23}$$

Putting $A = a^2$, $B = b^2$ in eqn. (13) and (14), we have

$$2BB'' - B'^2 - 1 = 0 \tag{24}$$

$$\frac{A''}{A} + \frac{A'B'}{AB} + \frac{1}{B^2} = 0 \tag{25}$$

Using the transformation

$$B = b^2 = \alpha\tau^2 + \beta\tau + \gamma \tag{26}$$

in (24), we get

$$4\alpha\gamma - \beta^2 = 1 \tag{27}$$

Using (26) in eqn. (25), we get

$$\left(\alpha\tau^2 + \beta\tau + \gamma\right)A'' + \left(2\alpha\tau + \beta\right)A' = \frac{A}{\left(\alpha\tau^2 + \beta\tau + \gamma\right)} \tag{28}$$

Using the transformation

$$\left(\alpha\tau^2+\beta\tau+\gamma\right)\frac{dA}{d\tau}=\frac{dA}{d\Psi} \tag{29}$$

in eqn. (28), we get

$$\frac{d^2A}{d\Psi^2}=-A \tag{30}$$

which leads to

$$\sin^{-1}\frac{A}{\ell}=\Psi-2\tan^{-1}m \tag{31}$$

where ℓ, m are arbitrary constants and

$$\Psi=2\tan^{-1}(2\alpha\tau+\beta) \tag{32}$$

is obtained from (29).

Now eqn. (30) leads to

$$A=a^2=\frac{8\alpha^2\ell m\tau^2+4\alpha\tau\left(\ell+2\beta\ell m-\ell m^2\right)+(\beta-m)(1+\beta m)\,2\ell}{\left(1+m^2\right)\left(4\alpha^2\tau^2+4\alpha\beta\tau+\beta^2+1\right)} \tag{33}$$

where ℓ, m are arbitrary constants.

Hence the metric (1) reduces to the form

$$ds^2=-\frac{\left(1+m^2\right)\left(4\alpha^2\tau^2+4\alpha\beta\tau+\beta^2+1\right)}{8\alpha^2\ell m\tau^2+4\alpha\tau\left(\ell+2\beta\ell m-\ell m^2\right)+(\beta-m)(1+\beta m)\,2\ell}\,d\tau^2$$

$$+\frac{8\alpha^2\ell m\tau^2+4\alpha\tau\left(\ell+2\beta\ell m-\ell m^2\right)+(\beta-m)(1+\beta m)\,2\ell}{\left(1+m^2\right)\left(4\alpha^2\tau^2+4\alpha\beta\tau+\beta^2+1\right)}\,dx^2$$

$$+\left(\alpha\tau^2+\beta\tau+\gamma\right)dy^2+\left[\left(\alpha\tau^2+\beta\tau+\gamma\right)\sin^2 y\right.$$

$$\left.+\frac{8\alpha^2\ell m\tau^2+4\alpha\tau\left(\ell+2\beta\ell m-\ell m^2\right)+\left(\beta-m\right)\left(1+\beta m\right)2\ell}{\left(1+m^2\right)\left(4\alpha^2\tau^2+4\alpha\beta\tau+\beta^2+1\right)}\cos^2 y\right]dz^2$$

$$-\frac{2\left(8\alpha^2\ell m\tau^2+4\alpha\tau\left(\ell+2\beta\ell m-\ell m^2\right)+\left(\beta-m\right)\left(1+\beta m\right)2\ell\right.}{\left(1+m^2\right)\left(4\alpha^2\tau^2+4\alpha\beta\tau+\beta^2+1\right)}\cos y\,dx\,dz \tag{34}$$

Some Physical and Geometrical Features

The scalar of expansion (θ), the shear scalar (σ^2), the spatial volume V and the density (ε) are given by

$$\theta=\left[\frac{\left(8\alpha^2\ell m\tau^2+4\alpha\tau\left(\ell+2\beta\ell m-\ell m^2\right)+\left(\beta-m\right)\left(1+\beta m\right)2\ell\right.}{\left(1+m^2\right)\left(4\alpha^2\tau^2+4\alpha\beta\tau+\beta^2+1\right)}\right]^{1/2}$$

$$\left[\frac{2\alpha\tau+\beta}{\left(\alpha\tau^2+\beta\tau+\gamma\right)}+\frac{4\alpha^2 m\tau+\alpha\left(1+2\beta m-m^2\right)}{4\alpha^2 m\tau^2+2\alpha\tau\left(1+2\beta m-m^2\right)+\left(\beta-m\right)\left(1+\beta m\right)}\right.$$

$$\left.-\frac{4\alpha^2\tau+2\alpha\beta}{4\alpha^2\tau^2+4\alpha\beta\tau+\beta^2+1}\right] \tag{35}$$

$$\sigma^2=\frac{2}{3}a^2\left(\frac{b'}{b}-\frac{a'}{a}\right)^2$$

$$=\frac{2}{3}\left[\frac{\left(8\alpha^2\ell m\tau^2+4\alpha\tau\left(\ell+2\beta\ell m-\ell m^2\right)+\left(\beta-m\right)\left(1+\beta m\right)2\ell\right.}{\left(1+m^2\right)\left(4\alpha^2\tau^2+4\alpha\beta\tau+\beta^2+1\right)}\right]$$

$$\left[\frac{2\alpha\tau+\beta}{2\left(\alpha\tau^2+\beta\tau+\gamma\right)}-\frac{4\alpha^2 m\tau+\alpha\left(1+2\beta m-m^2\right)}{4\alpha^2 m\tau^2+2\alpha\tau\left(1+2\beta m-m^2\right)+\left(\beta-m\right)\left(1+\beta m\right)}\right.$$

$$+\frac{4\alpha^2\tau+2\alpha\beta}{4\alpha^2\tau^2+4\alpha\beta\tau+\beta^2+1}\Bigg]^2 \tag{36}$$

$$V=b^2a$$

$$=\left(\alpha\tau^2+\beta\tau+\gamma\right)\left[\frac{\left(8\alpha^2\ell m\tau^2+4\alpha\tau\left(\ell+2\beta\ell m-\ell m^2\right)+\left(\beta-m\right)\left(1+\beta m\right)2\ell\right.}{\left(1+m^2\right)\left(4\alpha^2\tau^2+4\alpha\beta\tau+\beta^2+1\right)}\right]^{1/2} \tag{37}$$

$$\varepsilon=a^2\left[2\frac{a'b'}{ab}+\frac{b'^2}{b^2}-\frac{1}{4b^4}\right]+\frac{1}{b^2}$$

$$\varepsilon=\frac{2\ell m\alpha+m^2+1}{(1+m^2)(\alpha\tau^2+\beta\tau+\gamma)} \tag{38}$$

Discussion

If there are no particles attached to the string i.e. particle density $\epsilon_p = 0$. Then a situation arises where energy density (ϵ) is equal to the string tension density (λ) (from $\epsilon_p = \epsilon - \lambda$). This is the case of geometric string considered by Stachel[6]. This condition is physically relevant in cosmic explanation.

The reality condition $\epsilon > 0$ is satisfied when $2\ell m\alpha + m^2 + 1 > 0$. There is a big bang in the model at $\tau = 0$. The scalar of expansion (θ) is monotonically decreasing for $\tau > 0$ and $\theta \to 0$ when $\tau \to \infty$. The model (34) represents shearing and non-rotating universe. Shear (σ) is non-zero for $0 \le \tau < \infty$. Since $\lim_{\tau\to\infty} \frac{\sigma}{\theta} \neq 0$. Hence the model (34) does not approach isotropy for large value of τ.

However, when $\tau \to 0$ then $\varepsilon = \dfrac{2\ell m\alpha+m^2+1}{\left(1+m^2\right)\gamma}$

The spatial volume (V) is finite at $\tau = 0$ and it becomes infinite when $\tau \to \infty$. $\varepsilon \to 0$ when $\tau \to \infty$. Thus the model is essentially empty universe when $\tau \to \infty$.

Acknowledgements

The authors thank the Director, IUCAA, Pune (India) for providing hospitality under Associateship programme where this research work was completed.

References

1. Zel' dovich, Ya. B. (1975) *Sov. Phys. JETP* **40** : 1.
2. Kibble, T.W.B. (1976) *J. Phys. A. : Math. and Gen.* **9** : 1387.
3. Vilenkin, A. (1982) *Phys. Rev. D.* **20** : 2082.
4. Letelier, P.S. (1979) *Phys. Rev. D.* **20** : 1294.
5. Letelier, P.S. (1983) *Phys. Rev. D.* **28** : 2414.
6. Stachel, J. (1980) *Phys. Rev. D.* **21** : 2171.
7. Banerjee, A., Sanyal, A.K. & Chakraborty, S. (1990) *Pramana – J. Phys.* **34** : 1
8. Chakraborty, S. & Nandy, G.C. (1992) *Astrophy. and Space-Science* **198** : 299
9. Chakraborty, S. (1991) *Astrophys. and Space-Science* **180** : 293.
10. Bali, R. & Dave, Shuchi (2001) *Pramana, J. Phys.* **56** : 513.

PROC. NAT. ACAD. SCI. INDIA, 73 (A), II, 2003

A note on dual series equations involving certain biorthogonal polynomials

S. K. RAIZADA and V. K. KHARE

Department of Mathematics and Statistics, Dr. R. M. L. Avadh University, Faizabad (U.P.) India.

Received March 14, 2002; Accepted May. 31, 2002

Abstract

The authors have considered a pair of dual series equations involving a pair of polynomials suggested by jacobi polynomials which are biorthogonal over the interval (–1, 1) and have obtained the unknown coefficients involved in the series equations. Their limiting case, leading to Konhauser biorthogonal polynomials have also been considered.

(Keywords : Dual series equations/biorthogonal polynomials)

Introduction

In potential theory, many mixed boundary value problems reduce to the problem of solving of some dual series equations involving classical orthogonal polynomials as its kernels.

In the same effort Srivastava and Panda[1] have considered the problem of solving, the following dual series equations involving Jacobi polynomials of different orders.

$$\sum_{n=0}^{\infty} A_n \frac{\left|\overline{(\gamma+n+\ell)}\right.}{\left|\overline{(\rho+n+\ell)}\right.} P_n^{(\alpha,\beta)}\left(1-\frac{2x}{c}\right) = f(x), \forall x \in \mathrm{I}_1 \qquad (1)$$

and

$$\sum_{n=0}^{\infty} A_n \frac{\left|\overline{(\delta+n+\ell+1)}\right.}{\left|\overline{(\sigma+n+\ell+1)}\right.} P_{n+l}^{(\alpha,\mu)}\left(1-\frac{2x}{c}\right) = g(x), \forall x \in \mathrm{I}_2 . \qquad (2)$$

Where, $c>0$, ℓ is an arbitrary non-negative integer, $f(x)$ and $g(x)$ are prescribed functions,

and

$$I_1=\{x : 0 \le x < y\},\ I_2 = \{x : y < x \le c\}, \tag{3}$$

and in general,

$$\text{Min } \{\alpha, \beta, \gamma, \delta, \lambda, \mu, \ell, \sigma\} > -1 \tag{4}$$

For this purpose Srivastava and Panda[1] used the technique, of Noble[2] with some modifications. The dual series equations (1) and (2) happened to be generalizations of those considered earlier by Lowndes[3], Noble[2] and Dwivedi & Trivedi[4].

Recently, Madhekar and Thakre[5] considered the biorthogonal system of polynomials $\left\{J_n^{(\alpha,\beta)}(x;k)\right\}$ & $\left\{K_n^{(\alpha,\beta)}(x;k)\right\}$ suggested by jacobi polynomials over the interval (–1, 1) with weight function $w(x) = (1-x)^{\alpha}.\ (1+x)^{\beta}$

We know that

$$J_n^{(\alpha,\beta)}(x;1) = K_n^{(\alpha,\beta)}(x;1) = P_n^{(\alpha,\beta)}(x) \tag{5}$$

Thus, in view of above, in the present paper the authors have considered the problem of determining the sequence $\{A_n\}$ satisfying the following dual series equations :

$$\sum_{n=0}^{\infty} A_n \frac{\overline{[\gamma+k(n+\ell)+1]}}{\overline{[\rho+k(n+\ell)+1]}} J_{n+\ell}^{(\alpha,\beta)}\left(1-\frac{2x}{c};k\right) = f(x), \forall x \in I_1 \tag{6}$$

$$\sum_{n=0}^{\infty} A_n \frac{\overline{[\delta+n+\ell+1]}}{\overline{[(\sigma+n+\ell+1]}} K_{n+\ell}^{(\lambda,\mu)}\left(1-\frac{2x}{c};k\right) = g(x), \forall x \in I_2 \tag{7}$$

Where $c > 0$, ℓ is an arbitrary non-negative integer, $f(x)$ and $g(x)$ are prescribed functions, and in general,

$$\text{Min } \{\alpha, \beta, \gamma, \delta, \lambda, \mu, \rho, \sigma\} > -1$$

The method employed to solve (6) and (7) shall be analogous to that of used by Srivastava and Panda[1] with necessary modifications.

In view of (5), the dual series equations (6) and (7) are generalizations of (1) and (2), considered by Srivastava and Panda[1], and hence are generalizations of those considered earlier by Lowndes[3], Dwivedi and Trivedi[4].

It is interesting to note that :

$$\lim_{\beta\to\infty}\left\{J_n^{(\alpha,\beta)}\left(1-\frac{2x}{\beta c};k\right)\right\} = Z_n^{\alpha}\left(\frac{x}{c};k\right) \tag{8}$$

and

$$\lim_{\beta\to\infty}\left\{K_n^{(\alpha,\beta)}\left(1-\frac{2x}{\beta c};k\right)\right\} = Y_n^{\alpha}\left(\frac{x}{c};k\right) \tag{9}$$

In particular, for $k = 1$

$$Z_n^{\alpha}(x\,;1) = Y_n^{\alpha}(x\,;1) = L_n^{(\alpha)}(x) \tag{10}$$

Following Konhauser[6], $Z_n(x\,;k)$ and $Y_n(x\,;k)$ are defined by relations :

$$Z_n^{(\alpha)}(x;k) = \frac{\Gamma(1+\alpha+kn)}{n!}\sum_{j=0}^{n}(-1)^j\binom{n}{j}\frac{x^{kj}}{\Gamma(1+\alpha+kj)} \tag{11}$$

and

$$Y_n^{(\alpha)}(x\,;k) = \frac{1}{n!}\sum_{i=0}^{n}\frac{x^i}{i!}\sum_{j=0}^{i}(-1)^j\binom{i}{j}\left(\frac{1+\alpha+j}{k}\right)_n \tag{12}$$

In view of (8) and (9), by suitably appealing to the principle of confluence, our results in this paper would readily yield the corresponding results for dual equations involving series of Konhauser polynomials.

Preliminaries

We will use the following results which may be proved easily by use of differential recurrence relations :

(i) Fractional integrals :

$$\int_0^{\phi} x^{\alpha}(\phi - x)^{\mu-1} J_n^{(\alpha,\beta)}\left(1-\frac{2x}{c};k\right)dx$$

$$= B(1+\alpha+kn,\mu)\phi^{\alpha+\mu} J_n^{(\alpha+\mu,\beta-\mu)}\left(1-\frac{2\phi}{c};k\right) \tag{13}$$

and

$$\int_{\phi}^{c}\left(1-\frac{x}{c}\right)^{\beta}(x-\phi)^{\nu-1} K_n^{(\alpha,\beta)}\left(1-\frac{2x}{c};k\right)dx$$

$$= c^{\nu} B(1+\beta+n,\nu)\left(1-\frac{\phi}{c}\right)^{\beta+\nu} K_n^{(\alpha-\nu,\beta+\nu)}\left(1-\frac{2\phi}{c};k\right) \tag{14}$$

(ii) Derivative formulae :

$$D_x^m\left[x^{\alpha+m} J_n^{(\alpha+m,\beta-m)}\left(1-\frac{2x}{c};k\right)\right]$$

$$= \frac{\lceil(1+\alpha+m+kn)}{\lceil(1+\alpha+kn)} x^{\alpha} J_n^{(\alpha,\beta)}\left(1-\frac{2x}{c};k\right), m \geq 0 \tag{15}$$

and

$$D_x^m\left[\left(1-\frac{x}{c}\right)^{\beta+m} K_n^{(\alpha-m,\beta+m)}\left(1-\frac{2x}{c};k\right)\right]$$

$$=\frac{\left|\overline{(\beta+m}+n+1\right)}{(-c)^m\left|\overline{(\beta+n}+1\right)}\left(1-\frac{x}{c}\right)^{\beta} K_n^{(\alpha,\beta)}\left(1-\frac{2x}{c};k\right), m>0 \qquad (16)$$

(iii) The biorthogonality property in slight modified form :

$$\int_0^c x^{\alpha}\left(1-\frac{x}{c}\right)^{\beta} J_m^{(\alpha,\beta)}\left(1-\frac{2x}{c};k\right).K_n^{(\alpha,\beta)}\left(1-\frac{2x}{c};k\right)dx$$

$$=\frac{c^{\alpha+1}k^n\left|\overline{(1+\alpha}+kn\right)\left|\overline{(1+\beta}+n\right)}{n!\left|\overline{(1+\alpha}+\beta+n\right)\left|\overline{(1+\alpha}+\beta+n+kn\right)}\delta_{mn}, \alpha,\beta>-1 \qquad (17)$$

Where δ_{mn} is the Kronecker delta. The above results can be proved easily by use of above results and following the method of Madhekar and Thakre[5].

Corollary of (17) :

$$\int_0^y x^{\alpha}\left(1-\frac{x}{c}\right)^{\beta} J_m^{(\alpha,\beta)}\left(1-\frac{2x}{c};k\right).K_n^{(\alpha,\beta)}\left(1-\frac{2x}{c};k\right)dx$$

$$+\int_y^c x^{\alpha}\left(1-\frac{x}{c}\right)^{\beta} J_n^{(\alpha,\beta)}\left(1-\frac{2x}{c};k\right).K_m^{(\alpha,\beta)}\left(1-\frac{2x}{c};k\right)dx=0 \qquad (18)$$

$$0\le y\le c$$

Where y is arbitrary.

proof : To prove (18), for m ≠ n we have, from (17)

$$\int_0^c x^\alpha \left(1-\frac{x}{c}\right)^\beta J_m^{(\alpha,\beta)}\left(1-\frac{2x}{c};k\right) K_n^{(\alpha,\beta)}\left(1-\frac{2x}{c};k\right)dx = 0 \tag{19}$$

Similarly

$$\int_0^c x^\alpha \left(1-\frac{x}{c}\right)^\beta J_m^{(\alpha,\beta)}\left(1-\frac{2x}{c};k\right) K_m^{(\alpha,\beta)}\left(1-\frac{2x}{c};k\right)dx = 0 \tag{20}$$

For $0 \le y \le c$ we add (19) and (20) and write it in following form :

$$\left\{\int_0^y x^\alpha \left(1-\frac{x}{c}\right)^\beta J_m^{(\alpha,\beta)} K_n^{(\alpha,\beta)}dx + \int_y^c x^\alpha \left(1-\frac{x}{c}\right)^\beta J_n^{(\alpha,\beta)} K_m^{(\alpha,\beta)}dx\right\}$$

$$+\left\{\int_0^y x^\alpha \left(1-\frac{x}{c}\right)^\beta J_n^{(\alpha,\beta)} K_m^{(\alpha,\beta)}dx + \int_y^c x^\alpha \left(1-\frac{x}{c}\right)^\beta J_m^{(\alpha,\beta)} K_n^{(\alpha,\beta)}dx\right\} = 0 \tag{21}$$

Put

$$\Omega(m, n; y) = \int_0^y x^\alpha \left(1-\frac{x}{c}\right)^\beta J_m^{(\alpha,\beta)} K_n^{(\alpha,\beta)}dx$$

$$+\int_y^c x^\alpha \left(1-\frac{x}{c}\right)^\beta J_n^{(\alpha,\beta)} K_m^{(\alpha,\beta)}dx \tag{22}$$

So that (21) can be written as :

$$\Omega(m, n; y) + \Omega(n, m; y) = 0 \qquad m \neq n$$

or,

$$\Omega(m, n; y) = -\Omega(n, m; y) = 0 \qquad m \neq n \qquad (23)$$

From (22), we notice that $\Omega(m, n; 0) = \Omega(m, n; c) = 0$

For $m \neq n$ and (23) holds for every arbitrary y, so we conclude that $\Omega(m, n; y) = 0$, for all $y \in [0, c]$.

This proves (18).

In view of (5) it is further to note that for k=1. (18) reduces to the modified orthogonality relation for jacobi polynomials, given by Srivastava and Panda[1], (18) shall be most useful property in our investigations :

Multiplying-Factor Technique

We multiply (6) by $x(\phi-x)^{m+p-1}$ where p is an arbitrary constant and m is a suitable non-negative integer, and integrate both sides with respect to x over $(0, \phi)$, then by use of integral formula (13), we obtain :

$$\sum_{n=0}^{\infty} A_n \frac{\overline{|\gamma + k(n+\ell)+1|}\,\overline{|[1+\alpha+k(n+\ell)]|}\,\overline{|(m+p)}}{\overline{|[\rho+k(n+\ell)+1]|}\,\overline{|1+\alpha+m+p+k(n+\ell)]}}\phi^{\alpha+m+p} *$$

$$* J_{n+\ell}^{(\alpha+m+p,\beta-m-p)}\left(1-\frac{2\phi}{c};k\right) = \int_0^{\phi} x^{\alpha}(\phi-x)^{m+p-1} f(x)dx \qquad (24)$$

Now Diff. (24) both sides m times w.r.t. ϕ, we get by use of (15) :

$$\sum_{n=0}^{\infty} A_n \frac{\overline{|[\gamma+k(n+\ell)+1]|}\,\overline{|[1+\alpha+k(n+\ell)]}}{\overline{|[\rho+k(n+\ell)+1]|}\,\overline{|[1+\alpha+p+k(n+\ell)]}} J_{n+\ell}^{(\alpha+p,\beta-p)}\left(1-\frac{2\phi}{c};k\right)$$

$$= \frac{\phi^{-\alpha-p}}{\overline{|(m+p)}} D_{\phi}^{m}\left\{\int_0^{\phi} x^{a}(\phi-x)^{m+p-1} f(x)dx\right\} \qquad (25)$$

Where $0 < \phi < y$, $\alpha > -1$ and $m + p > 0$

Now when we multiply (7) by $\left(1-\frac{x}{c}\right)^{\mu}$ and differentiate the resulting equation i times with respect to x, then using formula (16), we obtain :

$$\sum_{n=0}^{\infty} A_n \frac{\overline{|(\delta+n+\ell)+1)|(\mu+n+\ell+1)]}}{\overline{[\sigma+n+\ell+1)|(\mu-i+n+\ell+1)]}} \frac{\left(1-\frac{x}{c}\right)^{\mu-i}}{(-c)i} K_{n+\ell}^{(\lambda+i,\,\mu-i)}\left(1-\frac{2x}{c};k\right) \tag{26}$$

$$= D_x^i\left\{\left(1-\frac{x}{c}\right)^{\mu} g(x)\right\}$$

Where i is a non-negative integer.

Now multiplying (26) by $(x-\phi)^{h+i-1}$ and integrating both sides with respect to x over the interval (ϕ, c) and using the formula (14) we obtain :

$$\sum_{n=0}^{\infty} A_n \frac{\overline{[\delta+n+\ell+1]|[\mu+n+\ell+1)]}}{\overline{[\sigma+n+\ell+1]|\mu+h+n+\ell+1)]}} K_{n+\ell}^{(\lambda-h,\,\mu+h)}\left(1-\frac{2\phi}{c};k\right)$$

$$= \frac{(-1)^i c^{-h}}{|(h+i)} \left(1-\frac{\phi}{c}\right)^{-\mu-h} \int_{\phi}^{c} (x-\phi)^{h+i-1} D_x^i\left\{\left(1-\frac{x}{c}\right)^{\mu} g(x)\right\} dx \tag{27}$$

Where $y < \phi < c$, $\mu - i > -1$ and $h + i > 0$.

Now if p and h are so choosen that the coefficients of $j_{n+\ell}^{(\alpha+p,\,\beta-p)}$ and $K_{n+\ell}^{(\lambda-h,\,\mu+h)}$ become identical and these polynomials are of the same order, then by applying (17) and (19), unknown coefficients $\{A_n\}$ can be determined. Below we discuss all such situations of interest :

The special Case $\rho = \alpha$ and $\sigma = \mu$

In the special case $\rho = \alpha$ and $\sigma = \mu$, we get, $p = \gamma - \alpha$ and $h = \delta - \mu$, the equations (25) and (27) reduce to the form :

$$\sum_{n=0}^{\infty} A_n J_{n+\ell}^{(\gamma,\delta)}\left(1-\frac{2\phi}{c};k\right)=\frac{\phi^{-\gamma}}{\overline{|(\gamma-\alpha+m)}}D_{\phi}^{m}\left[\int_0^{\phi} x^{\alpha}(\phi-x)^{\gamma-\alpha+m-1}f(x)dx\right] \quad (28)$$

and

$$\sum_{n=0}^{\infty} A_n K_{n+\ell}^{(\gamma,\delta)}\left(1-\frac{2\phi}{c};k\right)=\frac{(-1)^i c^{\gamma-\lambda}}{\overline{|(\gamma-\lambda+i)}}\left(1-\frac{\phi}{c}\right)^{-\delta} *$$

$$*\left[\int_{\phi}^{c}(x-\phi)^{\lambda-\gamma+i-1}D_x^i\left\{\left(1-\frac{x}{c}\right)^{\mu}g(x)\right\}dx\right] \quad (29)$$

provided that

$$\alpha + \beta = \gamma + \delta = \lambda + \mu$$

Now appealing to (17), (18) and (30), we get our result contained in :

Theorem : For $c > 0$, let the sequence $\{A_n\}$ be defined by the dual series equations (6) and (7).

Then for integers i, m, $\delta \geq 0$

$$A_s=\frac{(\delta+\ell)\overline{|[\alpha+\beta)+(\delta+\ell)(k+\ell)+1]}\overline{|(\alpha+\beta+\delta+\ell+1)}}{c^{\gamma+1}k^{\delta+\ell}\overline{|[\gamma+k(\delta+\ell)+1]}\overline{|(\beta+\delta+\ell+1)}} *$$

$$*\left[\frac{1}{\overline{|(\gamma-\alpha+m}}\int_0^{y}\left(1-\frac{\phi}{c}\right)^{\delta}K_{\delta+\ell}^{(\gamma,\delta)}\left(1-\frac{2\phi}{c};k\right)F(\phi)d\phi\right.$$

$$+\frac{(-1)^i c^{\gamma-\lambda}}{\overline{|(\lambda-\gamma+i)}}\int_y^c \phi^{\gamma} j_{\delta+\ell}^{(\gamma,\delta)}\left(1-\frac{2\phi}{c};k\right)G(\phi)d\phi\Bigg] \tag{31}$$

Where for convenience,

$$F(\phi)=D_{\phi}^{m}\left\{\int_0^{\phi} x^{\alpha}(\phi-x)^{\gamma-\alpha+m+1}f(x)dx\right\} \tag{32}$$

and

$$G(\phi)=\int_{\phi}^{c}(x-\phi)^{\lambda-\gamma+i-1}D_x^i\left\{\left(1-\frac{x}{c}\right)^{\mu}g(x)dx\right\} \tag{33}$$

Provided that (30) holds and

$$\alpha+\beta+1>-1,\ \gamma+m>\alpha>-1,\ \delta>\mu-i>1 \tag{34}$$

This theorem reduces to that of Srivastava and Panda[1] for $k = 1$ and hence also generalises to that corresponding results of Dwivedi and Trivedi[4].

References

1. Srivastava, H. M. & Panda, R. (1978) *Nederl. Akad. Wetensch. Proc. Ser. Math* **81(4)** : 502.
2. Noble, B. (1963) *Proc. Cambridge Philos. Soc.* **59** :363.
3. Lowndes, J. S. (1969 *Proc. Edinburgh Math. Soc. Ser.* **16(II)** : 273.
4. Dwivedi, A. P. & Trivedi, T. N. (1974) *Proc. Ser. Indag Math.* **36** : 203.
5. Madhekar, H. C. & Thakare, N. K. (1982) *Pacific J. Math* **100** : 417.
6. Konhauser, J. D. E. (1967) *Pacific J. Math* **21** : 300.

PROC. NAT. ACAD. SCI. INDIA, 73 (A), II, 2003

Experimental investigations of neuronic shaped planar microstrip patch and array antennas

DEEPAK BHATNAGAR[+], MANISHA GUPTA, JASWANT SINGH, VIJAY JANYANI* and RAJ. KUMAR GUPTA

Microwave Laboratory, Department of Physics, University of Rajasthan, Jaipur-302004, India.

**Department of Electronics and Communication Engineering, Malaviya National Institute of Technology, Jaipur-302017, India.*

[+]*Author for correspondence.*

Email : dbhatnagar_2000@rediffmail.com; FAX : (0141) 2702645

Received October 17, 2001; Revised September 5, 2002; Accepted Sep. 28, 2002

Abstract

Results of an experimental study, carried out on radiations from neuronic shaped planar microstrip patch and array antennas are presented in graphical from. It is concluded from this study that by applying scale-modelling principle on such radiators, radiation properties of human brain neurons can be estimated.

(**Keywords :** microstrip antenna/neurons/radiations from brain/ scale-modelling principle)

Introduction

The radiation properties of microstrip antennas have been extensively studied in recent years due to their practical advantages over conventional antennas including their lightweight, ability to conform to the host object and relatively easy and inexpensive fabrication compared to other antennas[1-3]. Earlier work related with radiation properties of microstrip antennas was limited to microstrip patches of regular shapes particularly rectangular, circular, triangular or elliptical geometries. In recent years, interest of scientific community has started shifting towards the analysis of

planar arbitrary shaped microstrip antennas[4-6] by applying different mathematical approaches.

Human body in general contains more than 10^{11} neurons and most of them are concentrated in human brain and eyes[7,8]. The sizes of these neurons vary from 0.02 micrometer to 100 micrometer or more. The shape, size, dimensions and properties of neurons differ from one portion of the brain to other. Most of the neurons are made of conducting materials. Due to continuous variation in the concentration of sodium, potassium, calcium and chlorine ions in brain, positive and negative voltages of intensity varying from –70 milli to approximately +60 milli volts are constantly generated[9]. It is worth mentioning here that in recent times, these voltages have been amplified thousands of time and are used in a device known as "MIND SWITCH" which is proving useful for handicapped and severely disabled persons. With the help of this device, these people can now operate electronic and electrical devices by using only brain signals without moving any part of his/her body[10-11]. When these alternating positive and negative voltages are applied to conducting neurons, they generate electromagnetic waves whose frequency depends upon the shape and other parameters of the neurons. In the same way, these neurons receive electromagnetic waves of appropriate frequency if available in the surrounding. Some AC signals of brain frequency spectrum have been measured by available instruments and found them in the range of few hertz. The voltages produced by these signals have been used to obtain Electroencephalography (EFG) signals from the brain[12].

The concept of designing of neuronic patch microstrip antennas (NPMA) to analyse the radiation and reception behaviour of human brain neurons was developed from two dimensional photographs of human brain neurons. The shape of a neuron of human hippocampus as seen by Barinaga[13], is similar to an irregular patch antenna. Human neurons have three-dimensional geometry but at this stage of work , to simplify our problem we have considered their cross-section only and developed them as microstrip patch antennas having small thickness. By applying scale modelling technique[14-15], dimensions of the cross section of a human brain neuron are converted into an antenna structure capable to operate in *C* band of electromagnetic frequency spectrum. However the thickness of neuron is not scale modeled due to non-availability of dielectric substrates of different thickness in local market, which are required for fabrication of microstrip antennas. This is perhaps the first reported work on NPMA structure hence scope for incorporation of third dimension *i.e.* thickness of neurons exist for future work to get more realistic picture regarding radiation performance of human neurons. This study on the radiation properties of neuronic antennas can be proved helpful in improving the performance of devices like "Mind

switch" etc. by indicating the direction of maximum intensity and nulls of the radiation patterns of brain radiators.

Design Details and Results

There are several shapes of neurons found in human brain[16]. The dimensions of human brain neurons are so small that an antenna structure with exact dimensions of an actual neuron cannot be fabricated for experimentation. Considering this fact, scale modelling principle[14-15] is applied and dimensions of cross section of a human neuron are increased so that neurons may be visualised as neuronic microstrip antennas with resonant frequency lying in *C*- band (4 to 8 GHz). The geometry with coordinate system of one such neuronic microstrip antenna developed in our laboratory is shown in Fig.1(a). The patch is located on one side of dielectric substrate (glass epoxy) while a very thin copper layer lies on other side of the substrate as ground plane. The substrate thickness is considered to be h and relative dielectric constant ε_r. The thickness of neuron (along z axis) is not scale modelled in the present paper. In fact, human body has hundreds or thousands of neurons associated in complicated three-dimensional networks. Instead of preparing a network at this stage of work, we initially prepared and observed the behaviour of simple two-dimensional linear and planar array arrangements of neuronic patch antennas. A two elements array of neuronic patch microstrip antennas as shown in Fig. 1(b) and a 2x2 elements planar array of similar antennas are also prepared for the present study. Both patch as well as array antennas are designed on a commercially available glass epoxy substrate (ε_r = 3.55) having 4' x 4' ground plane.

Several approaches are available to analyse arbitrary shape structure [4,5,17]. In the absence of regular boundaries, most of the techniques in general, are either based on rigorous mathematical treatments or they require sophisticated simulation software. Theoretical investigations of regular shape microstrip antennas require equivalent outward extension to incorporate the effect of fringing fields at the peripheries of the patch[18]. The extension depends upon the planar dimensions of the patch, substrate thickness, substrate relative permittivity and field distribution at its peripheries. It is difficult to estimate the extension at the peripheries of an arbitrary shaped patch. Palanisamy and Garg[17] proposed that for a given irregular shape, extension parameter available for a shape, closest to that of given shape could be used. The extension parameter involved with a rectangular geometry is well known[18]. Therefore a rectangular geometry OABC as shown in Fig. 1(a) just fitting outside the designed neuronic patch is considered to incorporate extension in different directions.

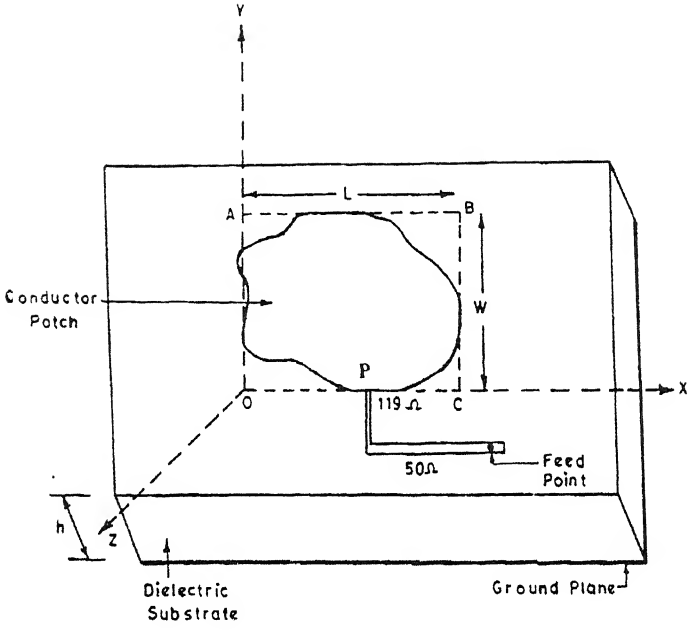

Fig. 1(a)–Single elements neuronic patch antenna with coordinate system.

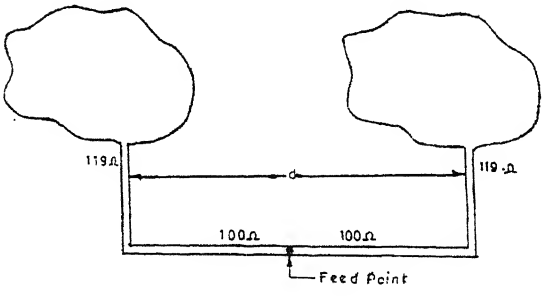

Fig. 1(b)–Two elements neuronic array antenna with feed network.

The length L of this rectangle OABC is 2.0 cm while width W is 1.2 cm. The substrate thickness h and substrate relative permittivity ε_r, applied for the present analysis are 0.16 cm and 3.55 respectively. The computed extension parameter ΔL is 0.469cm. By applying a computer programme named 'DEEREK. CPP' prepared in Window-95 based C^{++} programming language, analysis of this rectangular geometry is carried out by applying Model Expansion Technique[19]. Any point on the periphery of rectangular patch can be used to feed it if a suitable (λ / 4) transformer is attached between that point and feed line. Therefore point 'P', shown in Fig. 1(a), lying on the periphery of rectangle OABC may be used for feeding this rectangular structure. The computed input impedance (Z_{in}) of this rectangular antenna structure at point 'P' is (119.1 + j 2.87) ohm while its computed radiation efficiency is 79.11%. An argument similar to that of Palanisamy and Garg[17], regarding extension parameter of arbitrary shape structures, can be also be made here for searching the feed location on a neuronic patch antenna. The argument used in this paper is that for feeding a given irregular shape, feed location available for a shape, closest to that of given shape could be used. It can be seen from Fig. 1(a) that rectangle OABC just touches the neuronic patch at the point 'P' (1.10 cm, 0). Therefore point 'P' is used for feeding NPMA structure. For this purpose, computed input impedance of equivalent rectangular patch antenna (Z_{in}) at point 'P' is equated equal to that of a NPMA structure. To match this input indepdance with that of feed line (50 ohm), a (λ / 4) transformer is designed and attached between point 'P' and the feed line. The designing of this transformer and computation of width of feed lines is carried out by applying another computer programme 'DEEOSA. CPP' prepared by using the relations of ε_{eff} and Z_c discussed by Bahl and Bhartiya[18]. Feed arrangements for two elements array structure and 2 x 2 elements planner array antenna are designed following the same procedure. For two elements array structure, feed arrangements is shown is Fig. 1(b). All the structures are fed through SMA coaxial connectors and 50-ohm coaxial line. The measured E-plane ($\phi = 0°$) radiation pattern of NPMA structure is compared with that of its equivalent rectangular microstrip antenna (RMA) structure Fig. 2. These two patterns are nearly alike in nature. Both structures have maximum radiation intensity in end-fire direction ($\phi = 0°$). The measured 3dB beam width of NPMA structure is 70° as shown in Fig. 2, which is significantly smaller than that of RMA structure (110°) computed under identical conditions.

The radiation patterns, return loss, resonance frequency and input impedance of both neuronic patch as well as its arrays are measured at "Communication Systems Group, ISRO Satellite Centre, Bangalore" and "CARE IIT, New Delhi". The return loss, resonance frequency and input impedance measurements are carried out by using

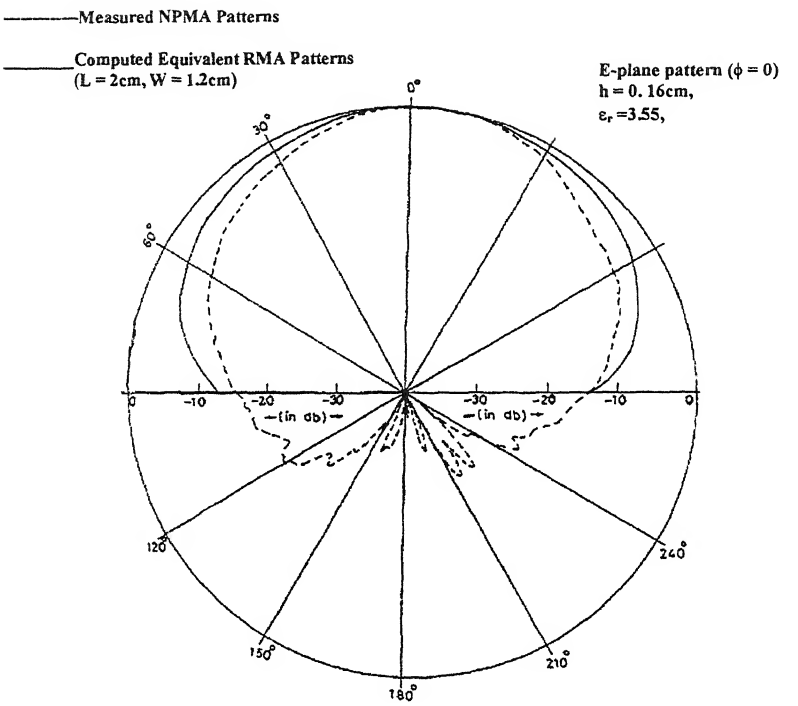

Fig. 2–Comparison between measured *E*-plane patterns of NPMA structure and computed *E*-plane pattern of its equivalent RMA structure.

a Vector Network Analyser and its associated computer programmes. During impedance measurements, due consideration was given to the accuracy enhancement techniques[20] to correct effective directivity, effective source match and frequency tracking errors. The measured resonance frequency of patch antenna using network analyser is around 6.68 GHz, which is little higher than that of its equivalent rectangular microstrip antenna (5.89 GHz). The measured return loss for a neuronic patch antenna is (–12.48) dB at 6.68 GHz as shown in Fig. 3(a) while the computed return loss of its equivalent rectangular microstrip antenna is (–17.77) dB at 5.89 GHz. The variation of return loss with frequency for two elements array and 2 x 2 elements planar array are shown in Fig. 3(b) and 3(c) respectively.

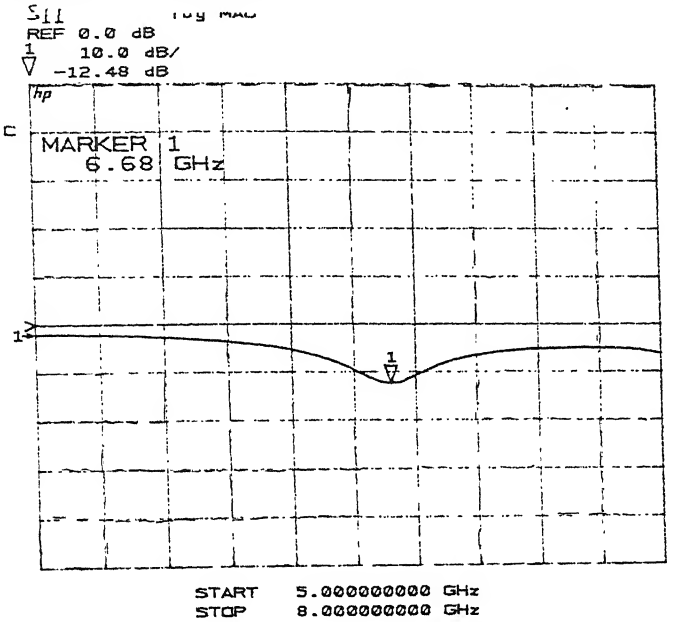

Fig. 3(a)–Measured return loss of a neuronic patch antenna.

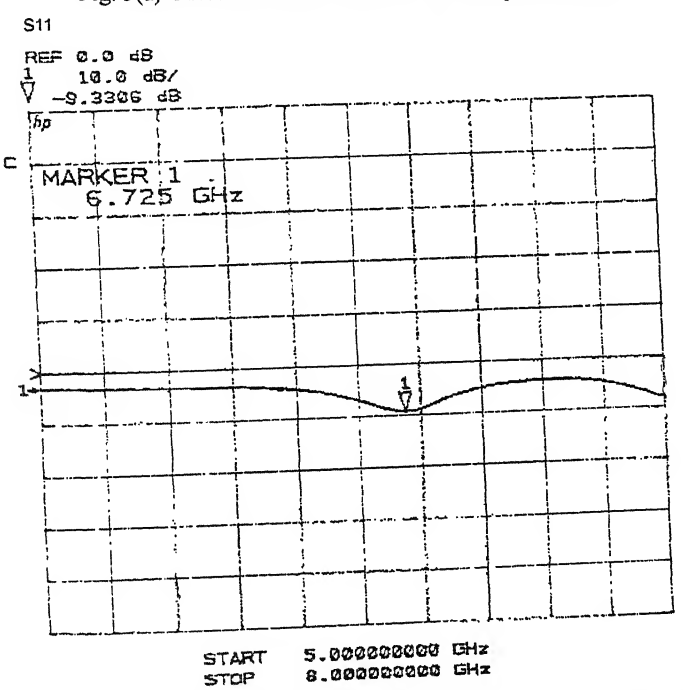

Fig. 3(b)–Measured return loss of two elements array of neuronic patch antennas.

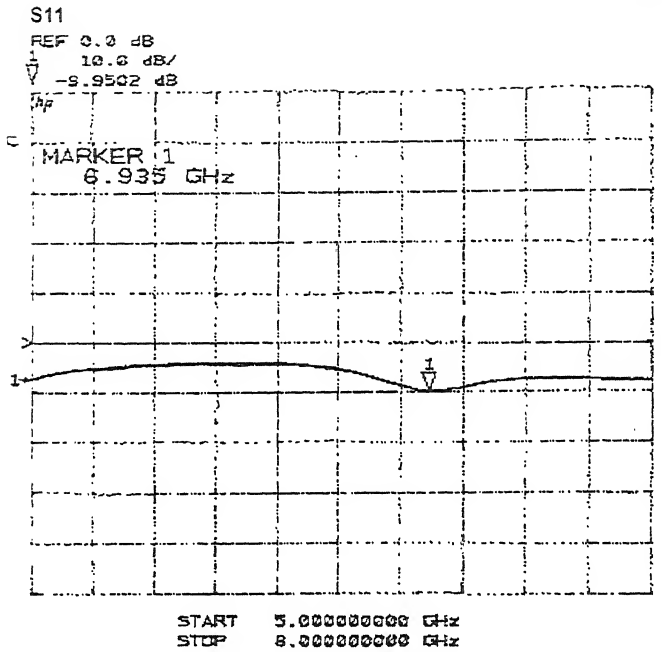

Fig. 3(c)–Measured return loss of 2 x 2 planar array of neuronic patch antennas.

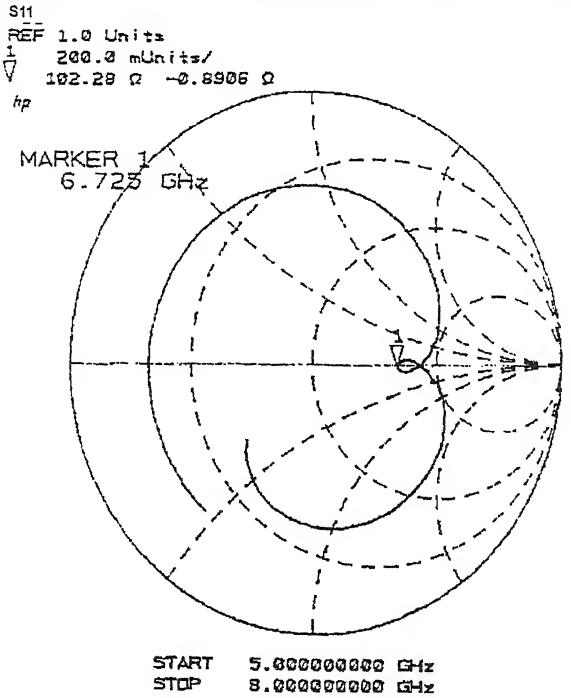

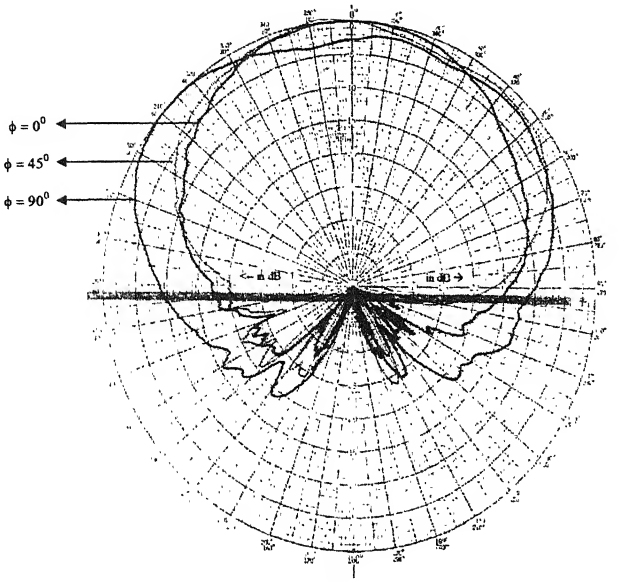

Fig. 5(a)

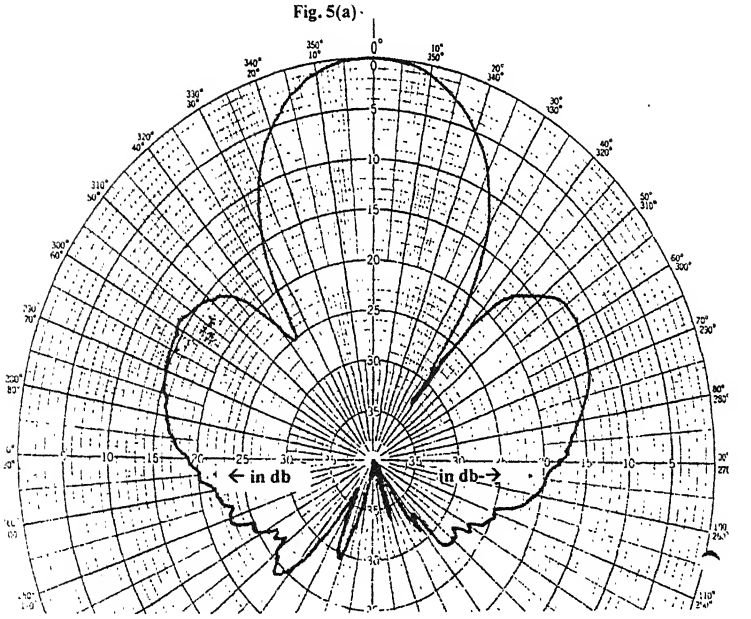

Fig. 5(b)

Fig. 5(a)–Radiation patterns of neuronic patch antenna with different ϕ planes.

Fig. 5(b)–*E*-plane radiation patterns of a two-elements array of neuronic patch antennas.

The measured resonance frequency for a two elements array is around 6.725 GHz while for four elements 2 x 2 planar array it is around 6.935 GHz. The measured input impedance for a two elements array as a function of frequency is shown in Fig. 4, which indicates a significant mismatch between radiating elements and feed network. The mismatch between radiating elements and feed network as well as difference in measured and computed resonance frequency and return loss values are on the expected lines since the feed network for NPMA structures is designed by considering smooth boundaries of regular rectangular patch antenna but in reality, the considered geometry of NPMA radiator bears an irregular shape though it is close to a rectangular shape.

The radiation patterns of NPMA structure and its two elements array are shown in Fig. 5(a) and 5(b) respectively. These patterns were measured by placing transmitting test antenna (NPMA) and fixed receiving horn antenna inside an anechoic chamber. The test antenna was mounted on an arrangement lying on a one-meter diameter circular wooden platform at ISRO Centre, Bangalore. The mount holding test antenna was capable in rotating in full range of colatitude angle (θ) varying from 0° to 360° and in different azimuthal (ϕ) planes. The separation between transmitting and receiving antennas was kept around two meters. With the help of a sweep generator, 6.68 GHz frequency signal was applied and radiation patterns for patch antenna were measured by changing angle θ from 0° to 360°. $\phi = 0$ and 90° pattern are sufficient to understand the radiation behaviour of NPMA structure. However radiation patterns plotted on polar graph are also reviewed in $\phi = 45°$ plane as shown in Fig. 5(a) to get three-dimensional feeling. The distribution of radiation intensity in upper hemisphere is quite similar for different ϕ planes. In $\phi = 0$ and 45° planes, maximum radiation intensity is in broadside direction while in $\phi = 90°$, maximum radiation intensity is in $\theta = 45°$ direction which are about 3dB more than that in $\theta = 0°$ direction. The radiations in lower half are due to surface waves generated by antenna, which are undesired radiations and needs to be suppressed. The radiation intensity in lower half is much smaller than that radiated in upper half. For a two elements array antenna, *E* plane radiation pattern is measured experimentally in $\phi = 0°$ plane at 6.725 GHz and is shown in Fig. 5(b). The main lobe in intensity distribution curve is again in broadside directions followed by side lobes. The side lobe level is about 15 dB down in comparison to the main lobe. Radiation intensity in lower half is again smaller than that radiated in upper half.

Discussion and Conclusion

Kirkup and co-workers[11] for the first time amplified the electromagnetic waves generated by human brain neurons in 1997 and found some interesting results in the

present communication, instead of observing radiations by actual human neurons, we have scale modelled the dimensions of a model of human brain neuron and converted it into a planar microstrip antenna operating in *C* band of frequency spectrum. Latter some planar arrays are designed and their radiation properties are measured experimentally. The expected radiation behaviour of human brain neurons is tried to explain with the help of measured data, of neuronic microstrip patch and array antennas.'

If we decrease the size of the modelled neuronic antenna to that of actual human brain neurons (0.02 micron to 100 microns), its effective frequency comes in the range of 10^{14} Hz. This is the frequency band of electromagnetic waves radiated by the Sun and other heavenly bodies and received on the earth after filtering through the electromagnetic windows around earth's atmosphere. The neurons of eyes receive these electromagnetic waves and convert them into respective colours using relevant portions of brain. In the same way, neurons of different parts of the brain also receive and generate electromagnetic waves whose frequencies correspond to the shape, size, dimension and other properties of the neurons.

The measured *E*-plane radiation patterns of a single neuronic patch microstrip antenna are drawn in Fig. 5a. These patterns are similar to those of other regular shaped microstrip antennas. Different ϕ planes are considered to visualize three-dimensional radiation patterns. It is observed that patterns are nearly uniform in all the directions. One can expect that in the same way human neurons might be radiating uniformly in all the directions. No back or side lobes are observed in measured radiation patterns of NPMA structure. Due to design considerations, NPMA structure can radiate only in upper hemisphere while an actual neuron will radiate in all the directions. The 3 dB beam width of neuronic patch antenna is little less than that of corresponding rectangular patch antenna operating under similar conditions. The measured *E* plane radiation pattern ($\phi = 0°$) of two elements neuronic patch array antenna excited in same phase is shown in Fig. 5b. The pattern has a well-defined main lobe followed by side lobes on both sides of main lobe. These side lobes are 12 to 14 dB down to the main lobe. The present model is a simplified model still one can have a feeling that human neurons arranged in complex three dimensional network might be radiating/receiving electromagnetic signals in/from the surroundings in a similar way.

The resonance frequency of a neuronic patch antenna is found 6.68GHz. It was expected that it would be significantly close to (5.89 GHz) *i.e.* of considered

rectangular patch antenna. The expectation was again based on the fact that geometry of designed neuronic antenna structure was nearly fitting into the considered rectangular patch geometry. However a significant deviation of 12% between observed and computed resonance frequency is recorded. In the same way, input impedance and return loss results are showing a significant mismatch between radiating patches and feed line. The reason behind this difference is that input impedance of NPMA structure at point 'P' is equated equal to that of its equivalent RMA structure and feed lines are designed accordingly. This arrangement is not found fully suitable for feed point selection. For proper matching between antenna and feed line, actual input impedance at point 'P' should be computed accurately by applying a simulation software and feed lines must be designed accordingly. Possibilities of error due to manufacturing limitations during designing of antenna structures cannot be ruled out.

As mentioned earlier, the signals generated by human brain neurons can be amplified several thousand times by means of a device now known as Mind Switch[10]. Research work in this direction is progressing[21-22]. The work will open possibilities of directing electromagnetic waves of particular phase and frequency towards a special part of brain and hence in modifying the behaviour of human being as brain neurons controls several characteristics of a person.

This is the first attempt, where expected radiation performances of a human brain neuron are observed by modelling it as planar microstrip patch and array structures operating at microwave frequencies. By applying available simulation software to locate correct feed point on antenna geometry and by designing several such radiating structures in the form of three-dimensional networks, more realistic results may be obtained.

Acknowledgements

The authors thank Dr. S. Pal, Deputy Director, DCA, ISRO Satellite Centre, Bangalore and Prof. B. Bhat, CARE, IIT, New Delhi, for permitting them to use experimental facilities available at their Centres. Authors also thank Mr. Santhil Kumar, ISRO Satellite Centre, Bangalore, for his help during the course of measurements and Ms. Rekha Lokwani and Dr. Osama Ali for their help in preparing computer programmes used in computation work.

References

1. Munson, R. E. (1974) *IEEE Trans.* **AP-22** : 74.
2. Carver, K. R. & Mink, J. W. (1981) *IEEE Trans.* **AP-29** : 1.

3. Post, R. E. & Stephenson, D. T. (1981) *IEEE Trans.* **AP-29** : 129.
4. Deshpande, M. D., Shively, D. G. & Cockrell, D. G. (1993) *NASA Technical Paper 3386, CECOM Technical Report.* **93E**-1 :1.
5. Mosig, D. G. (1988) *IEEE Trans.* **MTT-36** : 314.
6. Tsai, M. J., Flavis, F. D., Fordham, O. & Alexopoulos, N. G. (1997) *IEEE Trans.* **MTT-45** : 330.
7. Gupta, M. M. & Rao, D. H. (1994) *Neuro-control system,* IEEE Press, New York.
8. Gupta, M. M. & Knopf, G.. H. (1993) *Neuro-vision system,* IEEE Press, New York.
9. Gayton, A. C. (1991) *Textbook of medical physiology,* Prism Books (P) Ltd., Bangalore.
10. http:.//www.phys. uts.au/~asearle/mind_switch/media. html
11. Kirkup, L., Searle, A., Craig, A., McIsaac, P. & Moses, P. (1997) *Medical & Biological Engineering & Computing,* **35** : 504.
12. Berger, H. (1967) *EEG Clin. Neurophysiol. Suppl.* **28** : 1.
13. Baringa M, (2001) *Science Magazine* **291** : 2530.
14. Johnson, R. C. & Jasik, H. (1969) *Antenna Engineering Handbook,* McGraw Hill, New York.
15. Balanis, C. A. (1982) *Antenna Theory Analysis & Design,* John Wiley & Sons, New York.
16. Bourne, G. H. (1969) *The structure and function of neurons tissue,* Academic Press, New York.
17. Palanisamy, V. & Garg, R. (1986) *IEEE Trans.* **AP-34** : 1208.
18. Bhal, I. J. & Bhartia, P. (1980) *Microstrip Antennas,* Aretch House Inc., New York.
19. Carver, K. R. (1979) *Proc. Workshop on Printed Circuit Antennas,* New Mexico State Univ. : 7.01.
20. Hewlett Packard (1980) *Appl. Note* **AP-221A** : 5.
21. Rowe, D. G. (1998) *New Scientist* **160** : 5.
22. Craig, A., Kirkup, L., McIsaac, P., Dean, J., Searle, A., Tran Y. & Lal, S. (1997) *Proc. Thrid Australian Conference on Technology for People with Disabilities,* 125.

EDITORIAL ADVISORY BOARD

Reg. No. R.N. 35621/78

CONTENTS

Published by Professor H.C. Khare, General Secretary for the National Academy of Sciences, India, Allahabad and printed by National Graphics, Allahabad.
Managing Editor – Professor S. L. Srivastava